Phase behaviour in lipid tethers and vesicles - a thermodynamic study

Marie Lundgaard Guðmundsson

August 17, 2007

Preface

The work for this thesis was initiated in september 2006 at the Niels Bohr Institute, in the Membrane Biophysics Group. Starting out with a project description focused on building a simple FCS (Fluorescence Correlation Spectrometer), the project evolved and lead us to reconsider. During the initial experiments mainly meant as practise, it occurred that some of the "disturbing obstacles", tethers occurring when studying vesicles, were in fact interesting. Therefore my supervisor, Thomas Heimburg, and I decided to change the direction of my thesis. That is, instead of the construction of the FCS, the work was focused on the study of tether formation and a comparison between domain formation in vesicles and tethers.

There is a seemingly infinite number of interesting experiments to do in a further study of the topics covered in the present work. I have therefore strived to write a thesis that is both introductory in to the subject, and that hopefully can be used as an initial "how to" for students continuing experiments in this field.

I would like to thank to thank my supervisor Thomas Heimburg for good advice and encouragement when needed, and all of the Membrane Biophysics Group for their good company in the lab. Finally I would like to thank my friends and family for giving me their time and attention when ever I needed someone to listen to joys and frustrations during the work on my thesis. Special thanks should be given to Héðinn Björnsson for providing sharp deadlines during the last two months of work!

Abstract

In the proximity of melting transitions of artificial and biological membranes fluctuations in enthalpy, surface area, volume and concentration increase. These fluctuations leads to the formation of domains, changes of elastic constants and permeability and to longer relaxation processes. In this study fluorescence microscopy has been used to investigate domain formation in two-component unilamellar phospholipid membranes. The occurrence of domains in vesicles and tethers in the during phase transition has been studied and compared. It has been found that phase separation comparable to that of vesicles occur in tethers. In relation to the domain formation in tethers a method for automated detection and quantification of domains is proposed. The method invokes image filtering and Hough transformation to provide tether segment detection without time consuming manual detection.

Sammendrag

Nær en faseovergang i kunstige og narturligt forekommende membraner, er der store fluktuationer i entalpi, overfladeareal, volumen og tæthed. Disse fluktuationer danner gundlag for dannelsen at domæner, ændringer i elastiske konstanter og permeabilitet, samt længere relaksationstider. I det foreliggende arbedje er fluoresens mikroskopi blevet benyttet til at undersøge domæneformation i to-komponent, unilamellare membraner bestående af phospholipider. Dannelsen af domæner i vesikler og tuber er blevet studeret og sammenlignet, og det er vist at domæner kan dannes i tuber ligesom det kan i vesikler. I forbindelse med domæne dannelsen i tuber præsenteres en metode til automatisk detektering og analyse af domæner. Metoden benytter filtrering af billeder med en efterfølgende Hough transformering til en tidsbesparende detetktering sammenlignet med manuel analyse.

Contents

Chapter 1

Introduction

Phases and phase transition are phenomena that one knows from everyday life. The butter melts into liquid when removed from its cold shelter in the fridge to the hot frying pan. The ice cubes in a glass of whisky and soda disappear in the glass if one hesitates to drink. The water of a lake changes from swimming to ice skating lanes as the season turns from summer to winter. Taking a warm shower causes steam to form on the bathroom mirror. The spreading of salt on the pedestrian lane prevents it from turning into a slippery road to broken hips for senior citizens etc., and the list of phase transition phenomenas continues.

Basic science education in school introduces a more formal approach to these seemingly obvious consequences of changing temperature, and most schoolchildren will at some time melt ice over flames of burning gas, mix hot and cold water in little jars, heat metal blocks and thereafter plumb them into water to let them cool, etc. All this while filling in lab reports which are handed in to their teacher, and by the end of the year their work results in a grade. After this drill 14-year old children know words like "heat capacity", "phase transition" and "latent heat", and most of them can happily get on with their lives, whitout ever again having to bother about these concepts. Except for the ones that will some day find them selves studying chemistry, engineering or even physics. These haunted souls will again encounter these concepts, some of them even in the disguise of the branch termed "statistical physics". These children will grow up to build manufacturing plants, investigate obscure boson gases or run fancy breweries, all depending on their preferences.

For some reason education in thermodynamics, and scientific research using thermodynamics as toolbox, mainly deals with dead materials. Water,
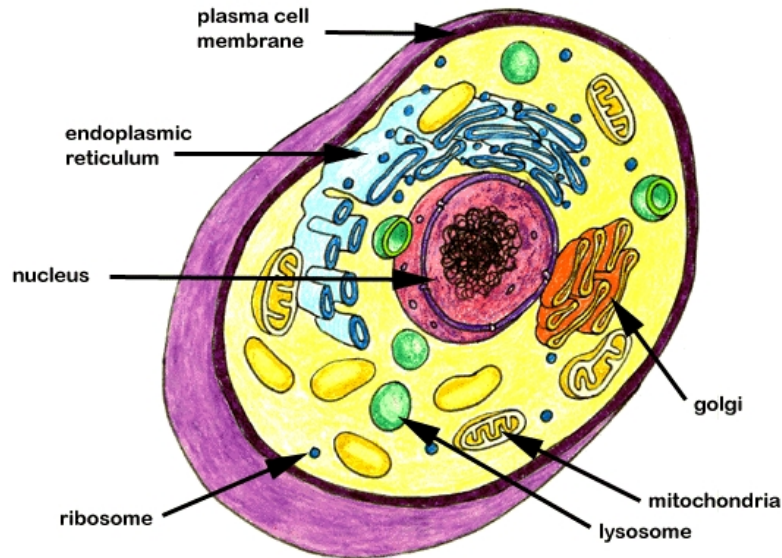
Figure 1.1: *Biological cell, [31]*

stones, chemical processes etc. But what about living organisms? What about bacteria, proteins, blood and even human cells? The thermodynamics of life itself have only been sparsely investigated.

This thesis deals with the thermodynamics of one of the brick stones of life: Fat. We will investigate phases and phase separation in artificial models of biological systems, balancing at the triple point between physics, biology and chemistry. In this introductory section the models and methods are presented and motivated in a non-academic form, suited for readers who want a brief and digestible presentation of the scope of the thesis.

1.1   The biological cell

One property shared by the vast majority of living organisms is the ability to define an "inside" and an "outside', and thereby distinguish between the organism and the environment. This feature is provided by the cell membrane, which exhibits rather sophisticated characteristics. While not only defining a border between exterior and interior of a cell, the membrane may also keep some substances inside the cell while letting others be transported to the
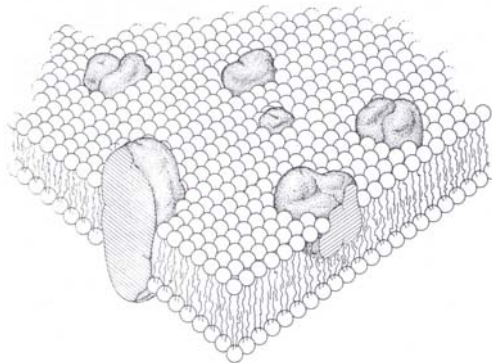
Figure 1.2: *Singer and Nicholsons model of the cell membrane [26]. Lipid matrix with floating proteins*

surrounding environment. Certain substances will be let to pass across the membrane, while others will be kept inside or outside. To give only a few examples, this may for instance allow an uptake of carbohydrates, release of neurotransmitters, and maintenance of gradients in ionconcentrations, pH-values etc. across the membrane.

A simplified example of an animal cell is given in figure 1.1. When examining living cells one finds that not only the morphological boundary is provided by a membrane, but also many of the organelles inside the cell are constituted of membranes. Among these are e.g. mitochondria, ribosomes, endoplasmic reticulum etc.

In 1972 Singer and Nicholson proposed a model describing the membrane, known as the "fluid mosaic model"[26]. It describes the cell membrane as consisting of a lipid bilayer, i.e. a double layer of fatty acids, within which a number of proteins are embedded, see figure 1.2. The model of Singer and Nicholson, with some refinements, still provides the basis for our understanding of the structure of the cell membrane.

1.2 Lipid model systems

Membranes occurring in nature consist of a variety of lipids and proteins, yielding complex characteristics which often prove to be difficult to extract and clarify. Thus artificial systems are advantageous to investigate, as they provide the possibility to construct much simpler systems than those found

in nature. This simplification may allow the experimenter to draw conclusions which may be extended to the more complex systems found in nature.

Lipids may undergo phase transitions. When the lipids of a lipid membrane "melts", the thickness of the membrane and diffusion times of proteins in this membrane are affected, among several other effects. It has been shown that the phase transition temperature is in a biologically relevant temperature regime, and one may therefore propose the idea that this has an effect of importance for biological organisms. It has furthermore been shown that phase separation may occur during the phase transition. That is, some areas may be thinner and less viscous than others.

In the present work the thermodynamic properties of two lipid bilayer structures - vesicles and tethers - are studied with regard to their phase transition and phase separation. While both structures have the same origin, the lipid bilayer, their different geometry makes them suitable as models for different systems. Yet both artificial vesicles and tethers can obtain sizes which can be observed using simple microscopy. The formation and structure of vesicles and tethers are explained in more detail in the Theory chapter, here only a brief description of vesicles and tethers shall be given.

1.2.1   Vesicles

Vesicles are spherical lipid bilayer structures, of which an example is given in figure 1.3. Phase separation in binary lipid vesicles leading to macroscopic structures was first reported in 1999 [4],[16], and has since the been the subject of a much research. Vesicles serve as good models for biological cells, and one may speculate that phenomenons comparables to the phase separation in artificial membranes may occur in biological cells too. Raft [14]

1.2.2   Tethers

While tethers like vesicles are constructed from the lipid biulayer, the tethers are thin, tubular structures, as opposed to the almost spherical veiscle strucutres. In nature they are observed as as interconnecting cells, and may be compared in size to nerve cells. Artificial tether networks very much resemble neuronal networks observed in nature, see figure 1.4. It has been suggested that they may serve as transport connections between cells[13]. The investigation of tethers are interesting both from the perspective of transport properties, but also in the perspective of them being models for nerves.
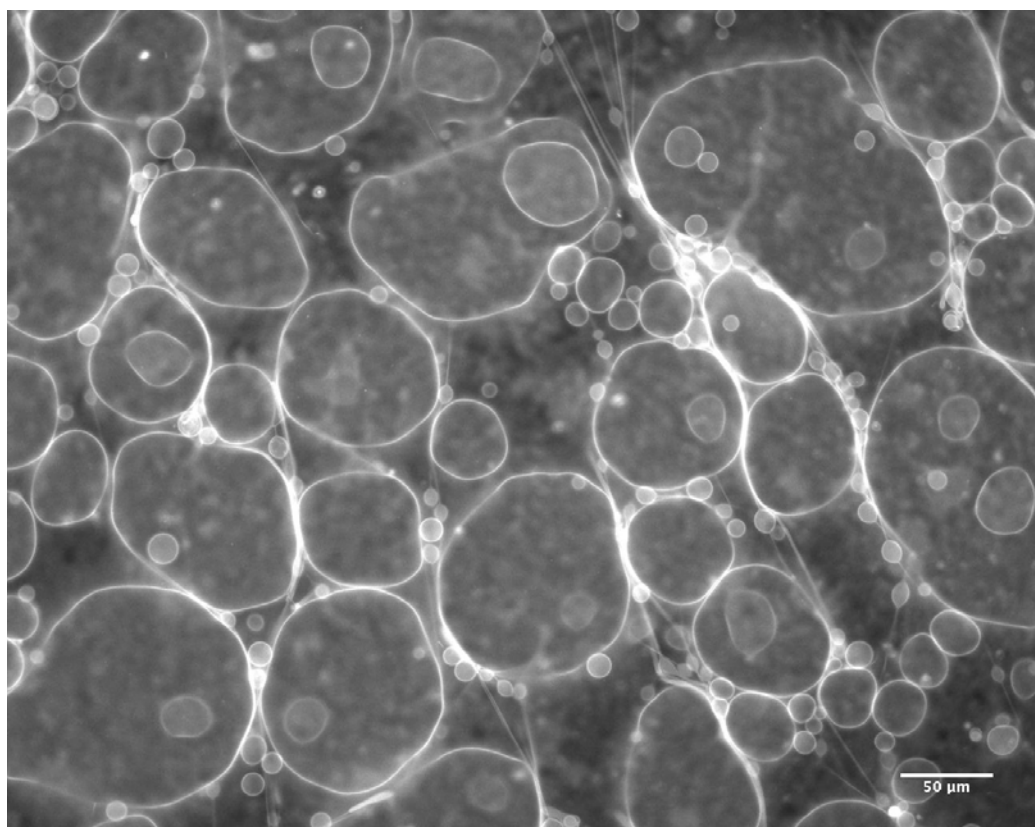
Figure 1.3: *Example of vesicles made from an artificial lipid bilayer. The size is camparable to that of bilogical cells, which in general lies in the rane 1-100μm*
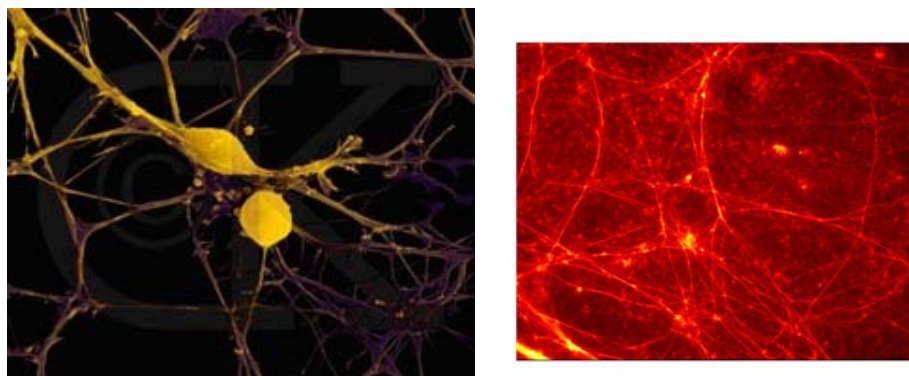
Figure 1.4: *Examples of naturally occuring and artificial lipid networks.***left:** *Image of a neuronal network* **right:** *A lipid network made from an artificial lipid network.*

In the present work the tethers are, as the vesicles, studied with regard to phase separation. This is especially interesting in the light of recent studies by Heimburg and Jackson[9], know as the Soliton Model. While it is beyond the scope of this work to go in to details on the Soliton Model, it should be mentioned that the phase separation in tethers are of great interest in the context of this work.

1.3 Image analysis

The vast majority of the data for this thesis are images. The images yields large amounts of information, and in order to increase the data processing time, it is advantageous to have a computer analyse the content. However this has proved to be a complex task. What seems obvious for the human eye proves to be complicated to translate in to a mathematical formulation suitable for computerised analysis. As an example, consider the puzzle in figure1.5. According to the manufacturer, this is suited for children age 1 year and older. Yet writing an algorithm that would make a computer solve the same problem would most likely be way more time consuming than letting the child do a dozen of them on its own.

Since this thesis requires the analysis of a large stack of images, the challenge of translating the obvious visual impression into a mathematical formulation had to be taken. As a part of this a special effort has been put in to the implementation of a procedure for automated image analysis of the tether

Figure 1.5: *Puzzle suited for children age +1 year.[6]*

pictures. The reason for this will be further motivated in the chapter on image analysis.

1.4 Motivation for the thesis work

The present thesis is focused on the study of phase separation in lipid systems. This is of interest as the lipid membrane shows distinct properties depending on physical state. Historically the proteins embedded in the membrane have been ascribed the major significance for the biological processes related to the cell membrane, and the lipids regarded as simply the matrix providing fixpoints for the proteins. In recent years though the lipid and their influence on various mechanisms have drawn attention. One may ask the question:

> "*Why not speculate, then, that phospholipids and their metabolites will soon be the subject of an information explosion, similar to that presently occurring for genes and proteins? The issues, problems, and methods necessary for such a development are upon us, starting with the ultimate physiological mystery of how membranes and, thereby, cellular life might have evolved.*"[10]

While I am not claiming to answer this "ultimate physiological mystery" in this thesis, I will investigate and compare the phase separation of phospholipid systems in two geometrically different configurations: (half)spheres and tubules/tethers. The work emphasise the thermodynamic properties of the lipid system, with perspectives drawn to possible roles in biology.

When observing the structures in the microscope the features and patterns of the structures are strikingly to the human eye and easy to detect, yet difficult to make a computer extract. A method for detection and characterisation

of domains in vesicles and tethers will be described. The problem of tether detection has only been described recently in 2006 by Hodneland et. al.[11]. The method presented here requires less information than the method by Hodneland. Further the method described here also treats the investigation of tether domains, an issue that to our knowledge have not been treated before. The mathematical/computerized treatment of images as opposed to a manual treatment saves valuable time for the scientist.

To summarise the scope of this thesis, what we want to study is:

- The relation, if any, between phase transition and macroscopic phase separation in artificial lipid membranes

- A comparison of phase separation in lipid tethers and vesicles

- A method for image acquisition of 3D structures using simple fluorescence microscopy

- A method for automated detection of tether segments

With the above in mind, the reader should now be able to read the rest of the thesis - or jump directly to the conclusion if in lack of time...

Chapter 2

Theory

In this section the underlying theory of this study is presented. It is intended as an introduction in to membrane thermodynamics, presenting the parts necessary to grasp the concepts of the present thesis.

The present work is focused on domain formation in two component lipid bilayers related to the enthalpy of the system. This chapter will therefore start out by considering the structure of lipids and the lipid bilayer, with an emphasis on the changes in these during a phase transition. Thereafter the theory necessary to understand mixing behaviour will be introduced.

2.1 The lipid bilayer

As described in the Introduction, the lipid bilayer is the basis for the cell membrane. In this section the lipid membrane will be described in more detail, along with its thermodynamic properties with special regard to the phase transition.
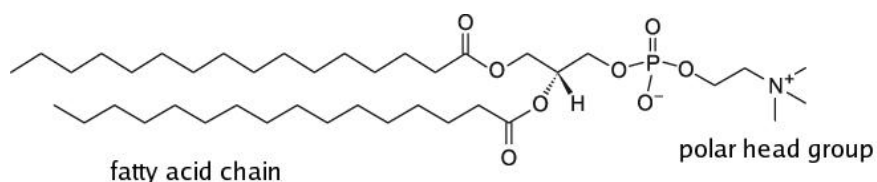
Figure 2.1: *Example of a phospho lipid. A glycerol backbone connects two fatty acid chains to a phosphate containing polar head group*

Lipid	Percentage of total lipid composition			
	Human Erythrocyte Plasma membrane	**Human** Myelin	**Beef** Heart Cell Mitochondria	**E. coli** membrane
Phosphatidic acid	1.5	0.5	0	0
Phosphatidylcholine	19	10	39	0
Phosphatidylethanoloamine	18	20	27	65
Phosphatidylglycerol	0	0	0	18
Phosphatidyllinositol	1	1	7	0
Phosphatidylserine	8	8	0.5	0
Sphingomyelin	17.5	8.5	0	0
Glycolipids	10	26	0	0
Cholesterol	25	26	3	0
Others	0	0	23.5	17

Table 2.1: *The lipid composition in different biological membranes [29]*
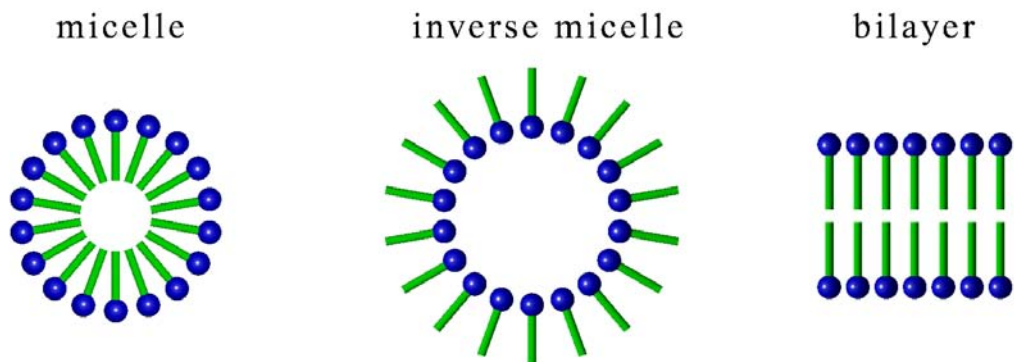
Figure 2.2: *Different lipid conformations. The blue spheres represent head groups, and the green sticks represents the two fatty acid chains*

The model systems investigated consists of phospholipids, a group of lipids often found in biological membranes, as may bee seen in table 2.1. Phospho lipids consist of fatty acid chains linked to a glycerol core with a phosphate group. An example of the structure is given in figure 2.1. The polar phosphate head group is hydrophilic whereas the tails are hydrophobic. A molecule containing both hydrophobic and hydrophilic groups are called amphiphilic, a property which comes in to play when dissolved in a polar media like water. When the amphiphilic lipids are dissolved in water the lipids may arrange in different structures, depending on lipid type. Examples of these are given in figure 2.2. These aggregates form as the nonpolar, hydrophobic tails try to avoid contact to water. In this thesis however, we shall be concerned only with structures based on the lipid bilayer.

The closed structures of interest in the present work divides in to two group, spherical structures called vesicles, and longer, elongated structures called tethers or tubules. The vesicles are classified according to their diameter:

20nm - 50 nm small

50nm - 500nm large

500nm - 300μm giant

The size of naturally occuring cells are in the range 1μm-100μm. The model systems investigated using microscopy for this work lies in the μm-regime, and are thsu comparable in size to biological structures.

2.1.1   The melting transition

The heat capacity is defined as

$$c = \frac{dQ}{dT},$$

(2.1)

letting Q denote heat and T denote temperature. With enthalpy defined as $H = U + PV$, one finds that at constant pressure the heat capacity can be written as

$$c_p = \left(\frac{\partial H}{\partial T}\right)_p$$

(2.2)

Integrating over the temperature interval of interest one finds

$$\triangle H = \int_{T_i}^{T_f} c_p dT \tag{2.3}$$

Now consider an ensemble of degenerate states. For such a system containing j states, the partition function is defined as

$$Z = \sum_j exp \left[-\frac{\triangle H_j}{kT} \right] \tag{2.4}$$

Now combining equations 2.2 and 2.4, and take the derivative with respect to temperature, one finds

$$c_P = \frac{< H^2 > - < H >^2}{RT^2} \tag{2.5}$$

Now consider this result. It tells that the higher the heat capacity of a system is, the higher the fluctuations in the enthalpy will be. Similar considerations on the relation between the heat capacity and the ensemble can be done in order to show that a number of other parameters are related to the heatcapacity in a similar way. On emay for instance show that the relaxation time for a system that is perturbed from equilibrium is given by

$$\tau = \frac{RT^3}{L} \cdot \triangle c_P \tag{2.6}$$

and that also the volume and area compressibility is affected,

$$\kappa_T = \frac{\bar{V}^2 - \bar{V}^2}{V \cdot RT^2}, \qquad \kappa_T^{area} = \frac{\bar{A}^2 - \bar{A}^2}{A \cdot RT^2} \tag{2.7}$$

That is, when the heat capacity of a system is large, the system undergoes fluctuations in several parameters. It has been shown that lipid systems follow this assumption [8],[25].

2.1.2 Phase transition of lipids and lipid membranes

In order to understand the structure and behaviour of a lipid membrane, an understanding of the single membrane components is required. The transition of the single lipid is linked to the conformational change of the tails. As the lipid melts, the tails curl up in response to the increased entropy and thus number of conformational states, see figure 2.3. During the phase transition the enthalpy is altered, T_t being the transition temperature. as

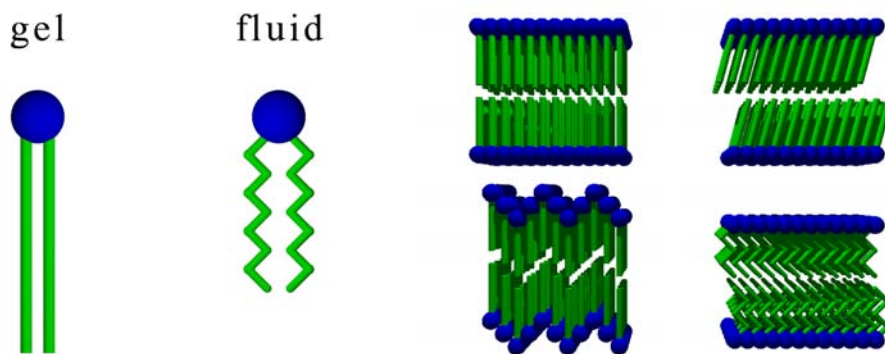$$\triangle H = \triangle S \cdot T_t \tag{2.8}$$

gel   fluid

Figure 2.3: *A single lipid in the gel* Figure 2.4: *Phases of the lipid bilayer.*
and fluid states.   **Upper row: L_β and L_c, Lower**
    row: $P\alpha$ and L_α

When considering the phase transition of the entire membrane one can-
not only stick to the single lipid approach. The transition of the membrane
is a cooperative process. The melting point is defined at the temperature at
which the number of lipids in the fluid state equals the number of lipids in
the gel state.

As the membrane lipids goes from the gel to the fluid state the thickness
of the membrane decreases, and the area per lipid increases. In addition to
the conformation of the single lipids, it turns out that also the orientation of
the molecules with regards to each other should be taken in to account. In
the gel state the lipids are arranged on a hexagonal lattice. The lipid bilayer
can assume different states depending on the temperature.The phases of the
lipid bilayers pictured in figure 2.4 are

L_β "gel" or "solid ordered" state. The lipid chains are highly ordered and
    tilted, and the lipids are arranged on a 2-dimensional lattice.

$P\alpha$ "ripple phase". The membrane in the ripple phase is mainly in the gel
    state, but shows line defects which are described as "ripples".

L_c crystalline phase.

L_α "fluid " or "liquid disordered" state. This state is characterised by dis-
    ordered lipid chains and random distribution of the lipids in the mem-
    brane plane.

In figure 2.5 an example of the excess heat capacity during a phasetransi-
tion is given. The two peaks is associated with the "pre-transition" in during
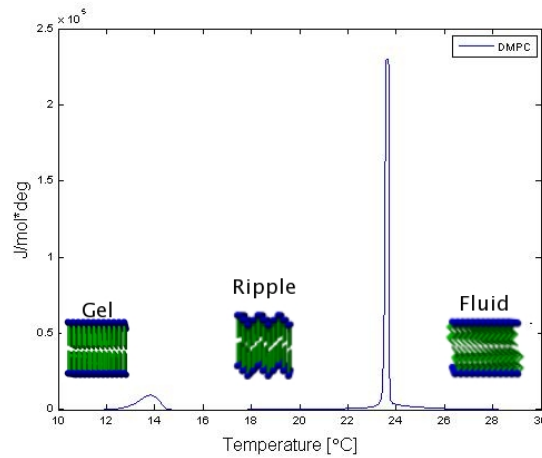
Figure 2.5: *An example of the excess heat capacity of a single component lipid membranes, with the associated conformations of the lipid bilayer.*

which the membrane changes from the solid-ordered to the ripple phase. The second, larger peak represent the main transition, i.e. the transition from the ripple phase to the liquid-disordered phase.

2.1.3 Proteins and dyes in the membrane

Proteins and dyes may integrate in the membrane. This is worth considering since in the experimental work of this study a fluorescent dye is inserted in the membrane. Insertion of proteins in the membrane may cause structural changes in the surrounding membrane. The consequences were first proposed in the socalled Mattress model by Mouritsen and Bloom[21]. The structural changes caused is seen in figure 2.6.

Structural changes

When a protein inserts in to the membrane, the surroundings change in order to minimise the energy. According to the model this causes proteins shorter that the membrane thickness to decrease the membrane thickness, while the opposite is the case for longer proteins.

Changes in phase transition profile

As a consequence of the changing membrane structure, the melting point of the membrane may be shifted to higher or lower temperatures. This is almost
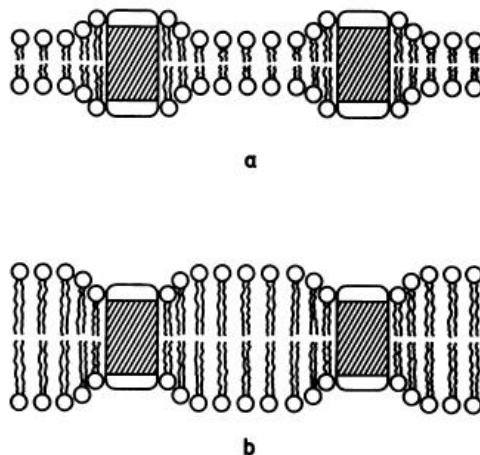
Figure 2.6: *The membrane response to the insertion of transmembrane proteins (**a**) longer or (**b**) shorter than the membrane thickness, as described by the Mattress model [21].*

intuitively understandable if one compares figures 2.3 and 2.6. One sees that the insertion of e.g. short proteins favors a decrease in the membrane thickness, a change also associated with the melting transition.

2.2 On mixtures and phase transitions

When considering the phase transition of a system, the phase diagram of the system may give information of the expected composition of the system at given conditions. The phase transition does not solely depend on the constituents of the system, but also on the physical structure/formation. That is, for at system with high cooperativity the transition range will tend to be narrower as changes to the system rapidly are distributed throughout the system.

Excess heat capacity of 1-component membranes and a binary mixture is presented in figure 2.7. What is wanted is a way to predict the phases of a binary lipid system under given curcumstances. In the following two approaches to describing the phase fraction of a 2-component system will be presented.

Figure 2.7: *Measured excess heat capacity curves. Pure DMPC, DPPC, and a 1:1 DMPC:DPPC sample.*
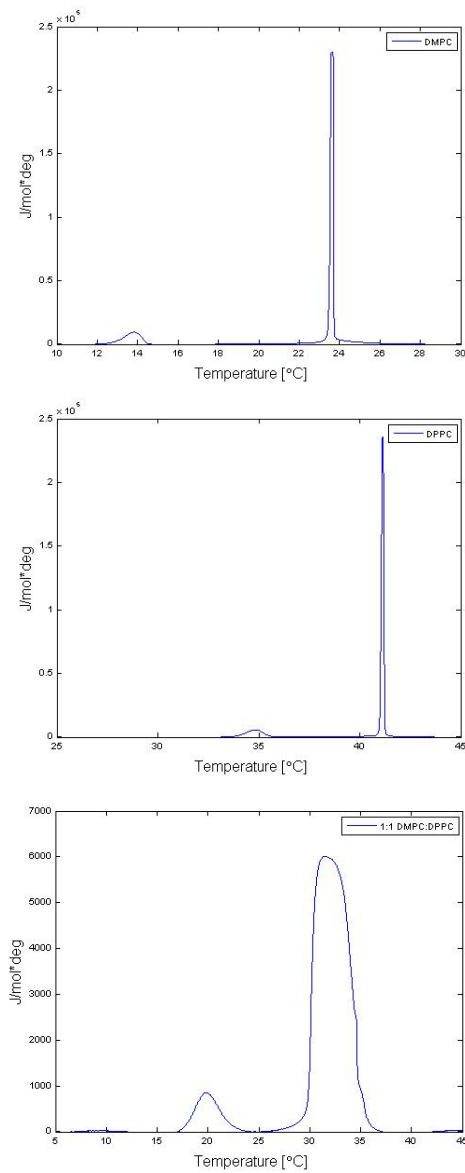
Ideal solutions

The phase diagram of lipid membranes was first proposed by Lee [17]. In an ideal solution one assumes a perfect mixing of the two components, i.e. the interaction of the different molecule species are the same. Assume the two species A and B, which can take the conformations f and g. In equilibrium one has that the chemical potential, μ, for the two species are equal

$$\mu_A^f = \mu_A^g \tag{2.9}$$

Let $\mu_x^{X,0}$ denote the Gibbs free energy of species X in the state x under standard conditions. Standard conditions shall be the temperature T and pressure 1bar. The chemical potentials are given as

$$\mu_A^g = \mu_A^{g,0} + RT ln \left(x_A^g\right) \tag{2.10}$$

$$\mu_A^f = \mu_A^{f,0} + RT ln \left(x_A^f\right) \tag{2.11}$$

Using the conditions for chemical equilibrium, eq. 2.2, one finds

$$ln \frac{x_A^f}{x_A^g} = \frac{-\mu_A^{f,0} + \mu_A^{g,0}}{RT} \tag{2.12}$$

Let the transition enthalpy be $\triangle(H_A)_T = H_A^{f,0} - H_A^{g,0}$. Now take the first derivative of Eq. 2.12, and find

$$\left(\frac{\partial ln \frac{x_A^f}{x_A^g}}{\partial T}\right) = \frac{H_A^{f,0} - H_A^{g,0}}{RT^2} = \frac{\triangle(H_A)_T}{RT^2} \tag{2.13}$$

Integrating from T_A to T, one finds

$$ln \frac{x_A^f}{x_A^g} = \int_{T_A}^{T} \frac{(\triangle(H_A)_T)}{RT^2} dT \tag{2.14}$$

considering the enthalpy for component A one finds

$$\triangle(H_A)_T = (\triangle H_A)_{T_A} + \int_{T_A}^{T} \triangle c_p dT = (\triangle(H_A)_{T_A} + \triangle c_p(T - T_A)) \tag{2.15}$$

Heat capacity difference between phases $\triangle c_p = 0$ gives

$$ln\frac{x_A^f}{x_A^g} = \int_{T_A}^{T} \frac{(\triangle(H_A)_T}{RT^2}dT \tag{2.16}$$

and further

$$ln\frac{x_A^f}{x_A^g} = -\frac{(\triangle(H_A)_{T_A}}{R}\left(\frac{1}{T} - \frac{1}{T_A}\right) \tag{2.17}$$

Now take the exponential of Eq. 2.17 in order to get

$$\frac{x_A^f}{x_A^g} = exp\left[-\frac{(\triangle(H_A)_{T_A}}{R}\left(\frac{1}{T} - \frac{1}{T_A}\right)\right] = e^{-A} \tag{2.18}$$

If one does the same calculations for the component B, one finds

$$\frac{x_B^f}{x_B^g} = exp\left[-\frac{(\triangle(H_B)_{T_B}}{R}\left(\frac{1}{T} - \frac{1}{T_B}\right)\right] = e^{-B} \tag{2.19}$$

and thus

$$A \equiv -\frac{(\triangle H_A)_{T_A}}{R}\left(\frac{1}{T} - \frac{1}{T_A}\right) \tag{2.20}$$

$$B \equiv -\frac{(\triangle H_B)_{T_B}}{R}\left(\frac{1}{T} - \frac{1}{T_B}\right) \tag{2.21}$$

Using

$$x_A^g = 1 - x_B^g \tag{2.22}$$
$$x_A^f = 1 - x_B^f \tag{2.23}$$
$$\tag{2.24}$$

along with Eq. 2.18 one finds for the fraction of species A in the state f

$$x_A^f = (1 - x_B^g)e^{-A} \tag{2.25}$$

Doing similar calculations for species B one finds

$$x_B^g = \frac{x_B^f}{e^{-B}} \tag{2.26}$$

Combining the two above equations leads to

$$x_A^f = \left[1 - \left(\frac{x_B^f}{e^{-B}}\right)\right] e^{-A} \tag{2.27}$$

and from this and Eq. 2.24 one finds

$$x_A^f = \left[1 - \frac{\left(1 - x_A^f\right)}{e^{-B}}\right] e^{-A} \tag{2.28}$$

Rearranging this gives

$$x_A^f = \frac{e^{-A}(e^{-B} - 1)}{e^{-B} - e^{-A}}. \tag{2.29}$$

Using again Eq. 2.24 one finds for the component B

$$x_B^f = \frac{e^{-B}(e^{-A} - 1)}{e^{-A} - e^{-B}}. \tag{2.30}$$

That leads us to the end

$$x_A^G = \frac{e^{-B} - 1}{e^{-B} - e^{-A}} \tag{2.31}$$

$$x_B^G = \frac{e^{-A} - 1}{e^{-A} - e^{-B}} \tag{2.32}$$

$$\tag{2.33}$$

These equations are used to predict the theoretical phase diagram for the binary mixture. The result is plotted in figure 2.8. The phase distribution can be found using the so called lever rule, explained in figure 2.8.

Regular solutions

The regular solution approach is necessary for systems in which the interaction parameters between the different species differs from each other. That is, the interaction energy between different species and and states are different, e.g. $E_{A,l} \neq E_{A,f}$. Consider a mixture of the to solutes A and B, with the chemical potential of A given by:

$$\mu_A = \mu_A^0 + RT ln\left(x_A \cdot j_A\right) \tag{2.34}$$

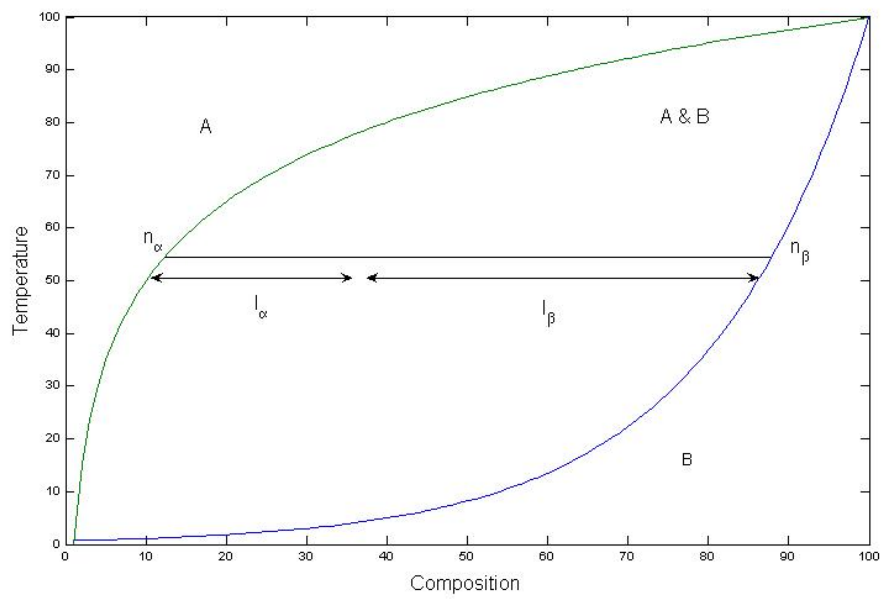The excess chemical potential is given as:

Figure 2.8: *Phase diagram of two phases A an B. The At a point in the two phase region of the diagram, the amount of the two phases may iin equillibrium be found as $n_\alpha l_\alpha = n_\beta l_\beta$*

$$\mu_A^R = RT \cdot ln(j_A) \tag{2.35}$$

The excess free energy for the interactions is found to be

$$G^R = x_A \cdot \mu_A^R + x_B \cdot \mu_B^R \tag{2.36}$$

Assuming thermodynamical equilibrium, i.e. $\mu_A^f = \mu_A^g$ and $\mu_B^f = \mu_B^g$, one finds

$$ln\frac{x_A^l}{x_A^g} + \frac{\rho_0^l \left(1 - x_A^l\right)^2 - \rho_0^g \left(1 - x_A^g\right)^2}{RT} = \frac{-\triangle H_A}{R} \cdot \left(\frac{1}{T} - \frac{1}{T_A}\right) \tag{2.37}$$

and

$$ln\frac{1 - x_A^l}{1 - x_A^g} + \frac{\rho_0^l \left(x_A^l\right)^2 - \rho_0^g \left(x_A^g\right)^2}{RT} = \frac{-\triangle H_B}{R} \cdot \left(\frac{1}{T} - \frac{1}{T_B}\right) \tag{2.38}$$

These equations cannot be solved analytically. A tool that have profed to provide solutions in agreement with experiemts is Monte Carlo simulation, and one can from that obtain values for $x_A^l, x_A^g, x_B^l, x_B^g$ The method of Monte Carlo simulation was first applied to lipid membranes by Sugar et al. [28]. Monte Carlo simulation has not been invoked in this thesis, but examples can be found in e.g. [7].

With the concepts introduced in this chapter, the reader should be able to benefit from the following description of experiments and results.

Chapter 3

Materials and Methods

This chapter will introduce the experimental methods used for studying the phase behaviour of the two component lipid systems.

3.1 Preparation of samples

The sample preparation for measurements in the calorimeter and in the microscope will be treated in the present section.

The lipid model systems studied in this work are prepared from lipids purchased from Avanti Polar Lipids (AL USA). The lipids used differ only in chain length. The dye used is is Di-C$_{18}$ (manufacturer number D-282), purchased from Molecular Probes/Invitrogen (Eugene, Oregon, USA). All lipids and the dye were used without further purification. Specification of used phospholipids and dye can be found in Table 3.1 and Table 3.2., respectively. The choice of the dye Di-C$_{18}$ will be motivated in Section 3.3.

All glassware and equipment used for the preparation of samples were cleaned using water, mucasol (a detergent) and ethanol and there after dried using nitrogen before use. All solutions were stored at -18°C in between measurements. Stock solutions were prepared by first weighing the lipids, and there after calculating and adding the amount of solvent needed for the desired concentration. Letting n denote mol, M$_w$ molecular weight and m mass, the needed amounts are straight forwardly calculated as

$$m = n \cdot M_w \tag{3.1}$$

and

$$n = c \cdot V \tag{3.2}$$

Phosholipid Abr.	Chain length	Melting point	Molecular weight
DLPC	12	-1°C	621.83 $\frac{g}{mol}$
DMPC	14	24°C	677.94 $\frac{g}{mol}$
DPPC	16	41°C	724.05 $\frac{g}{mol}$

Table 3.1: Specification of used phospho lipids. **DLPC**: Di Lauryl Phosphatidylcholine **DMPC**: Di Mirystoyl Phosphatidylcholine. **DPPC**: Di Palmitoyl Phosphatidylcholine

Dye	chain length	Abs. max	Emit. maxs	Molecular weight
DiI C_{18}	18	550nm	569	1052.08

Table 3.2: Specification of the used dye. The abbreviation Di-C_{18} is short for the full name: 1,1'-dioctadecyl-3,3,3',3'-tetramethylindocarbocyanine perchlorate.

The amount of lipid can be weighed with high precision, but due to practical reasons it is difficult to control the amount. The most efficient way to reach a given concentration is to take approximately the amount of needed lipid/dye, and thereafter determine the needed solvent.

3.1.1   Samples for calorimetry

Stock solutions of different lipids, i.e. DMPC, DLPC and DPPC, and of DiI C_{18} were prepared in chloroform, in concentrations of 10-20mM. From these solutions the samples were prepared in the acquired composition, e.g. 2mM 3:7 DLPC:DPPC, 1mol% DiI-C18. Upon sample preparation the chloroform is removed by first drying the sample under a stream of nitrogen, and thereafter leaving the sample under vacuum for a at least 2-3 hours. After the removal of chloroform water is added to the desired concentration.

3.1.2   Samples for microscopy

The sample preparation for microscopy is very similar to that of calorimetry. The only difference is that, after the removal of chloroform, Tri Fluor Ethanol (TFE) is added instead of water. This is the case as the surface tension of TFE is less than that for chloroform, thus fore providing a better spreading of the sample on the Indium Tin Oxide coverslips (ITO), see section 3.2.2..
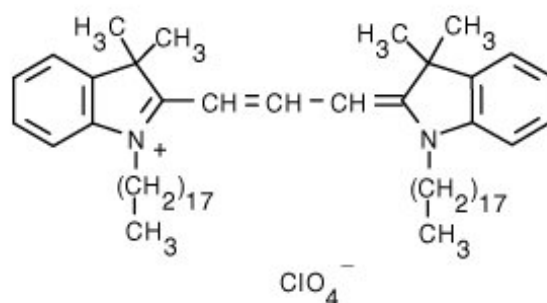
Figure 3.1: *structure of DiI C18*

3.2 Formation of giant unilamellar vesicles

Vesicle formation can be done using different approaches, but for the present case electroformation seems to be the most appropriate choice. It is a method with an acceptable success rate, as well as it can be done within a couple of hours. In the following two sections, the principle behind electroformation is described, as well as the experimental procedure.

3.2.1 Principles of electroformation

The method of electroformation has been used to produce vesicles. The method was first described by Angelova, 1986 [3], and provides a relatively fast and reliable method for formation of giant unilammellar vesicles (GUV). The principle is in short to form a lipid layer, place it in an aqueous solution, and thereafter apply an alternating electrical field. The procedure now utilises the charged head groups of the lipids, "dragging" or "pulling" halfspheres out of the lipid layer. See figure 3.2 for a simplified drawing of the effect

3.2.2 Procedure of electroformation

The chamber used is showed in figure 3.3. The chamber was made by the workshop at the Niels Bohr Institute, as a copy of a chamber previously used in the lab [5], with minor changes. In addition to this, a thick and a thin coverslip are used. The coverslips are covered with indium tin oxide on one side, making them conducting. The procedure for electroformation is as follows:
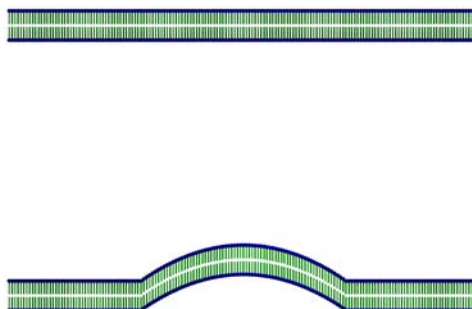
Figure 3.2: *A simplified drawing of the formation of GUV's by electroformation.* **Upper:** *lipid bilayer spread on ITO.* **Lower:** *Halfsphere pulled out of the planar lipid layer on the ITO.*
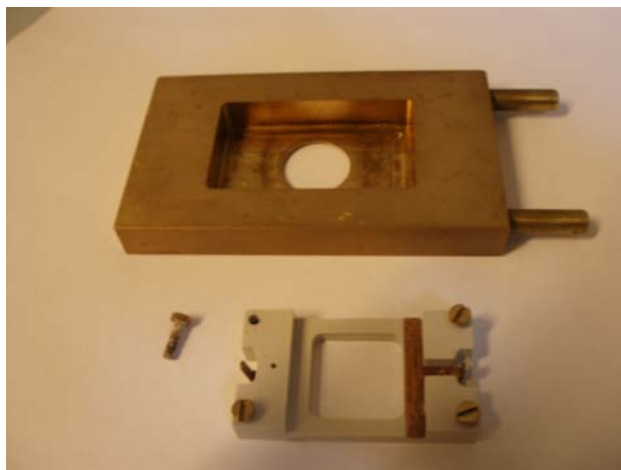

Figure 3.3: *chamber for vesicle formation*

- 4μl solution is applied to the conducting side of an ITO. The solution should spread circularly on the ITO in order to ensure formation of GUV's.

- the ITO is placed under vacuum for a few hours/over night, in order to remove excess liquid. The ITO is protected against light during this process.

- The lipid coated ITO is fastened to the bottom side of the plastic spacer chamber with vacuum grease. The plastic spacer is screwed onto the brass chamber.

- The chamber is now connected to a waterbath and heated to 60°C. When heated, preheated millipore water is added, and another, thicker, ITO is fastened on the upper side of the plastic spacer with vacuum grease.

- After appr. 15 min., when the lipid layer is assumed to be properly hydrated, a frequency generator is attached to the chamber. An alternating field of strength 2V and a frequency of 10Hz, of is applied for 15 min.

- The alternating field is turned off, and measurements of gel/fluid fraction can be initiated. Temperature can be controlled by the thermostat of the waterbath. Temperature measurements are conducted at waterdroplets placed on the upper ITO.

Following the above procedure has proved to be successful, i.e. to produce GUV's, in most cases, yet not always. See Appendix B for details, tips and tricks.

3.3   Microscopy

The vesicles produced by electroformation were observed using an inverted microscope. Olympus microscope, model IX71, using 20-100x air and oil objectives. The light source is a mercury lamp, passing through a band pass filter favouring the green colour on the excitatory side, and the orange on the emitting side.

The dye used, Di-C_{18} , is fluorescent with emission and absorption spectra as specified in table 3.2. The principle of fluorescence is as follows, with h being PLANCK constant, and *upsilon* denoting frequency. An atom is
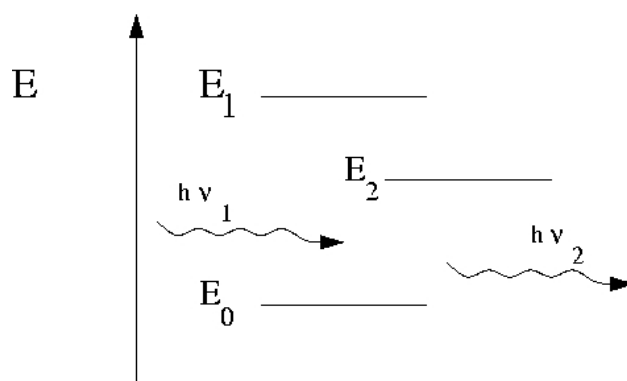
Figure 3.4: *The fluorescence principle. An atom is exited from its ground state of energy E_0 to the state E_1 by a photon of energy E_1. From E_1 it decays to the state E_2, and from there to E_0, emitting a photon of energy $h\upsilon_2$. The decay follows almost instantenaously after the excitation.*

exited by a photon of energy $h\upsilon_1$ from its ground state with energy E_0, to a state with energy E_1, $E_0 < E_1$, see figure 3.4. From this state it decays almost instantly through one or more internal transitions to the state E_2, and from here to the its ground state, emitting a photon with the energy $h\upsilon_2 = E_2 - E_0$. For the photon energies one finds that $h\upsilon_2 < h\upsilon_1$, and thereby the emitted light has a longer wave length than the excitatory light.

Figure 3.5 shows a principal drawing of the light path in the microscope. The white light from the mercury lamp is passed through a bandpass filter letting the orange light through. This light is passed tr hough the sample, there by exiting the fluorescent dye. When the exited atoms decays to the ground state, green light is emitted. This light may pass through a band pass filter favouring the green light, and may be observed through the eye pieces of the microscope, or detected by the CCD camera.

3.3.1 CCD camera

Pictures are made with a CCD camera which are mounted in the microscope. The camera is connected to a PC, and operated through the program Maxim DL. The camera is cooled to approx. -18°C prior to use in order to reduce thermal fluctuations, thus improving the image resolution. The CCD camera produces grayscale pictures with a resolution 1030x1300, in the format .tiff. An example is given in figure 3.6.
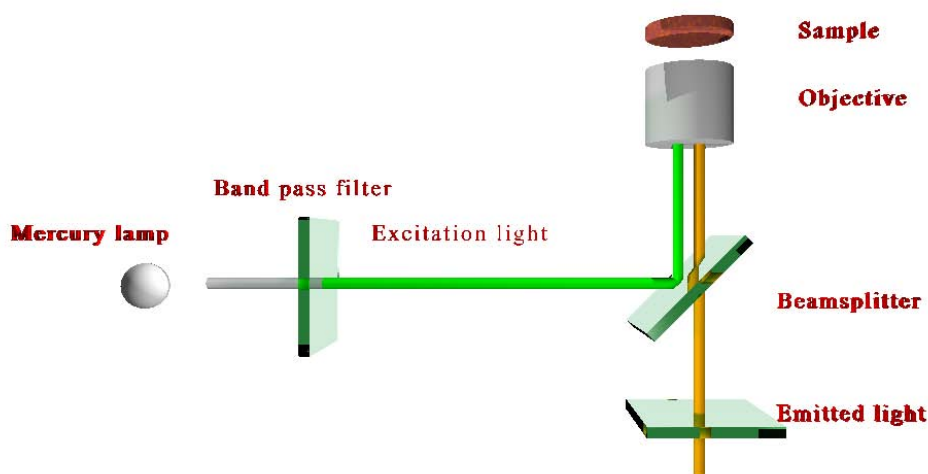
Figure 3.5: *The principle of the pathways of the light in the microscope. The light from the mercury lamp passes through a bandpassfilter favouring the green colour. The green light excites the Di-C$_{18}$, causing it to emit orange photons. These are passed through the beamsplitter, and may be observed via the eyepieces of the microscope.*

The vertical focus can be controlled via the focusing knobs on the microscope. Pictures are taken at different vertical positions in order to produce a 3D measurement of the vesicle and/or tether structure. The pictures are taken at vertical intervals of a few μm. Figure 3.7 shows different layers of a sample.

3.3.2 Measuring phase behaviour of lipid structures

The vesicle chamber was kept in connection with a waterbath during the observations in order to control the temperature of the sample. The upper side of the chamber was shielded with a block of insulating material, see figure 3.8, and the temperature of the chamber was controlled via a droplet of water on the surface of the upper ITO. The surface and internal temperature was assumed to be approximately the same. Temperature measurements inside the chamber has been conducted for calibration, using an upper coverslip with a small hole through which the thermocouple could be inserted.

Pictures were acquired at different vertical positions as described in the previous section. The chamber was left to equilibrate for at least 30min. between
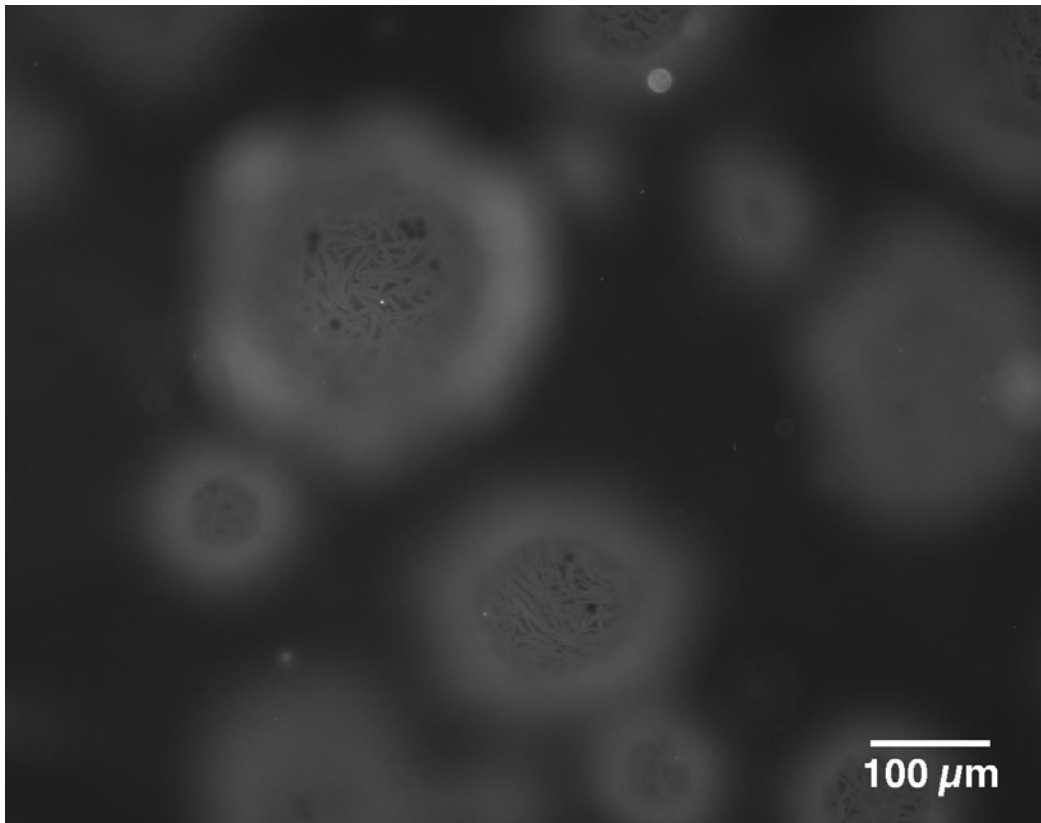
Figure 3.6: *A CCD picture taken at 32x magnification. The image show a 1:1 DMPC:DPPC mixture at 26,0° C . There is a profound domain formation.*
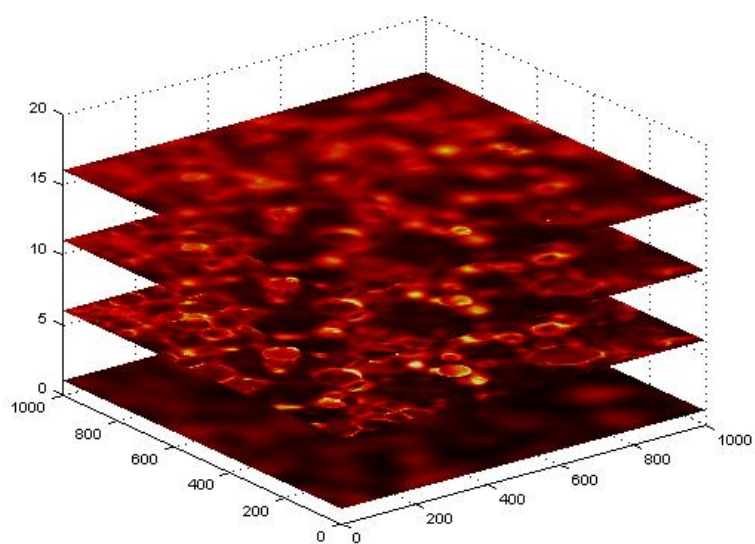
Figure 3.7: *3D layers shown for 1000x1000 pixel section ($\simeq 425\mu x425\mu m$). It demonstrate the sampling technique of sampling pictures at different vertical positions.*
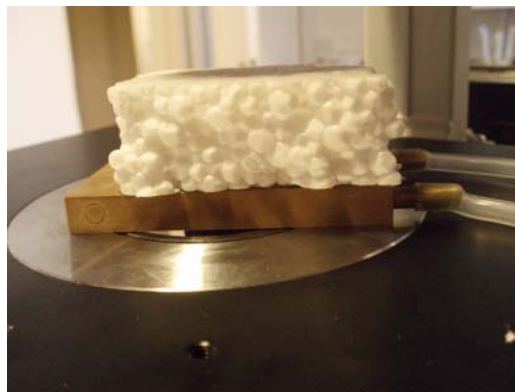
Figure 3.8: *The chamber used (see figure 3.3, during experiment. The block of insulationg material serves to lower the degreee of flows in the chamber, as well as it provides better temperature measurements via the water droplet on top of the upper ITO.*

each new temperature setting. This was done in order to ensure as homogeneous temperature distribution as possible, as well as allowing the lipid system to equilibrate.

Flows in the chamber

There occurred to be large temperature gradients in the chamber once the temperature of the chamber differed by more than 10°C from room temperature. These gradients produce flows which causes disturbances to the system under investigation. Especially tether measurements are disturbed by this, since small impurities and vesicles being washed around in the chamber gets caught in the tethers like flies in a spiders net.

Temperature measurement was performed at different positions in the chamber, inserting a thermocouple through a hole in the upper coverslip, as well as the temperature of the brass chamber was measured. These measurements showed relatively large temperature gradients inside the chamber. As much as 5°C over a distance of less than 1cm were observed for a thermostat temperature of 55°C. One therefore finds large temperature gradients inside the chamber, which may explain the large fluxes observed of lipid and solute inside the chamber. These large temperature gradients are both advantageous and disadvantageous: they produce the tethers which we want to study, corrupts a precise temperature measurement, and may disturb or even destroy the structures under observation, especially the tethers.
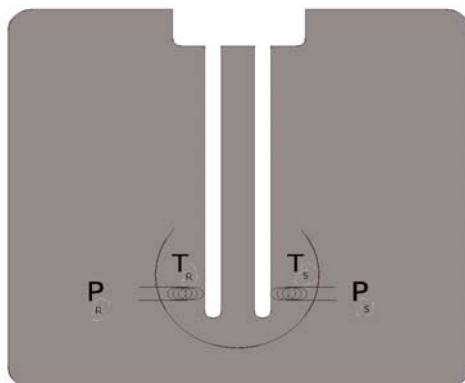
Figure 3.9: *Outline of the differential scanning calorimeter. Two identical cells, R and S, with separate heatings, P_1 and P_2.*

3.4 Differential scanning calorimetry

The calorimeter used is a differential scanning calorimeter, type VP-DSC, Microcal (Northampton/MA, USA). The calorimeter is operated via software provided by the manufacturer.

A schematic drawing of the interior of the calorimeter is given in see figure 3.9. The principle of the differential scanning calorimeter is as follows: Two cells, R and S, are adiabatically shielded from the surroundings. Their temperature is given by T_R and T_S. The two cells have separate heatings, denoted P_R and P_S. When measuring heat capacity profiles, one cell, S, is filled with sample solution while the other, R, is filled with a reference solution. When scanning through a given temperature range the temperature of the two cells are kept the same, and the calorimeter records the difference in power supply to the two cells.

The output from the calorimeter contains two columns; the temperature at a given time, and the corresponding difference in power supply to the cells, $\triangle P$. The excess heat is defined as:

$$\triangle Q = \int_t^{t+\triangle t} \triangle P(t')dt' \cong \triangle P \cdot \triangle t \tag{3.3}$$

During a phase transition the difference in power supply to the two cells will be significant, while it is close to zero for areas outside the transition regime.

Samples and reference solution are degassed under vacuum upon filling of the chamber in order to avoid disturbance from air bubbles. Heat capacity profiles of the samples are measured directly in the cells. The reference solution used in these experiments is millipore water, as the samples consists of lipids and millipore water. When filling the cells one use a long syringe which reach to the bottom of the cell. One has to be careful when filling the cells in order to avoid air bubbles. A tight lid is fastened on top of the cell, which causes the pressure to rise in the calorimeter cells. Thus prevents air bubbles to escape from the solution.

A number of parameters of the calorimeter scan are specified by the experimenter. Some of the more important are described in the following:

Start/Final temperature Start and end temperature of the scan. Should be chosen with a margin from the phase transition range. Most scans for this thesis were performed in the range 5°C to 50°C .

Scan rate The scanrate controls the rate at which the calorimeter scans through the temperature span. The scan rate is given in °C /hour. The faster the scan, the more uncertainty. Slow scanning require a strong sample solution in order to produce a detectable response. The scans for the present work were conducted at a rate of 5°C /hour.

Filtering Period The time interval at which measurement are done. The more diluted a sample is, the longer interval is needed in order to accumulate enough energy to detect. A filtering period of 10s was found to be appropriate.

Post/Prescan Thermostat lets the sample equilibrate before and after a scan. A period of 20 min. was chosen for the present work, in order to ensure an equilibrated system upon measurement.

Heat capacity profiles are presented in the Results section. The samples investigated in the microscope does not perfectly resemble the ones investigated in the calorimeter. The size of the vesicles differ, as well as the multilamellar vesicles are much smaller than the GUV in the vesicle chamber. Yet given the lack of precision in temperature measurements in the chamber, this is sufficient for the analysis of the given data.

Chapter 4

Theory of image analysis

Since a major part of the output of the experimental work for the present thesis is in the form of images, appropriate methods for extraction of data from these images has to be developed. There is a number of programs available for image analysis, but in most cases one has to tailor these to the specific needs of the particular task. In this section the theory underlying the computational procedures used for extraction of data from the pictures of tethers and vesicles will be described. The programs implementing the theory are listed in Appendix C, and may also be downloaded from www.nbi.dk/~lundgard.

For the present work, two problems have to be solved;

- Detection of the gel and fluid domains in vesicles, and an analysis of the fractional composition of gel and fluid domains.

- Detection of the gel and fluid domains in tethers, an analysis of the fractional composition of gel and fluid, and an analysis of the distribution pattern of domains within the particular tethers.

Where the two structures, vesicle and tether, have the same origin, a lipid bilayer, their different geometry requires different approaches. The vesicles are approached as 2 or 3 dimensional structures, whereas the tethers are considered as 1 dimensional, i.e. lines. In order to solve the two problems stated above, one has to chose suitable methods of filtering and segmentation, which will be described in this section.

I have furthermore developed a routine for automated detection of tethers and their gel and fluid segments. This will be compared to a manual detection and evaluated. The automated routine will be well suited for further investigations in the field, providing a fast method of data quantification.

That is, large amounts of information can be extracted and evaluated in reasonable time, providing faster progress.

4.1 Pictures

The pictures of tethers and vesicles are made using the CCD camera, as described in the Materials section. The image analysis has been done using Matlab, as this provides a good combination of predefined tools and algorithms, along with the possibility of user definition of routines. Further more Matlab is very suitable for building problem specific routine scripts which can easily be applied to a larger number of data files - in the present case image files. The computational speed of the transformations and image manipulation could very likely have been increased by using a lower level language such as C, but the faster programming time of Matlab caused me to choose this language instead. Additionally, Matlab provides a number of built in functions for image analysis, as well as it is easy to build graphical user interfaces.

4.1.1 From layers to a 2D projection

Pictures of the samples were taken in layers. These have been merged in order to obtain a pictures of the visible part of the vesicle. See fig 4.1 for an example of a vesicle picture made by merging. Margin has been done by performin a maximum intensity projection. That is the maximum value was found for each pixel along the Z-axes.

I have chosen not to perform this projection for the tether pictures. The merging causes slight a blurring of the pictures, which for the thin tether structures are profound compared to that of the vesicles. As a good resolution of the tethers are required in order to determine the domain sizes, the analysis is performed on one layer pictures.

4.1.2 Filtering of images

In order to extract the needed information from the CCD pictures, the conversion from gray scale pictures to a binary representation is advantageous. The images all contain noise caused by impurities in the chamber, different levels of illumination caused by clustering of dye containing lipids or different thickness of the lipid layer, as well as motion of the sample caused by flows in the chamber. The last factor yields a considerable contribution to the noise
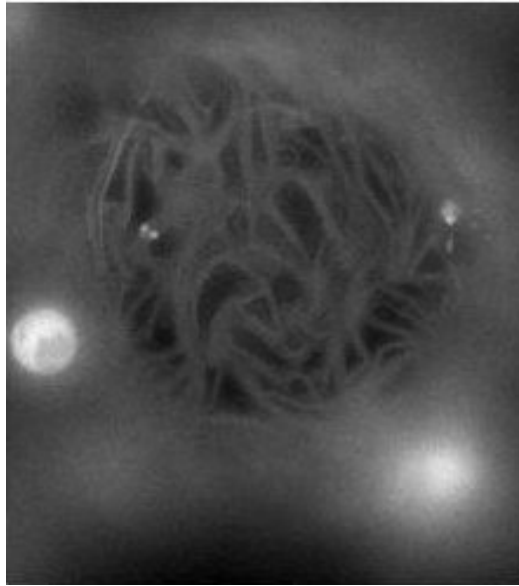
Figure 4.1: *Picture of a vesicle obtained by mergin of CCD images*

in the image data. When merging several pictures into one picture, the time delay of apr. 1 second between the capture of each image may corrupt the merged result.

By choosing a proper filtering method one may overcome some of the obstacles caused by the noise in the pictures. In the ideal

The method for tether detection presented by Hodneland et al. [11] is based on two image channels, where the one only detects the cells (compare: vesicles). But as this is not possible with our experimental procedure, I have chosen to generate artificial background.

The noise have been removed by the generation of an artificial background image, and subtracting this from the original image. The artificial background is generated for each image. A method often used in image analysis for this step, is to add a random/gaussian noise to the image, blur the image, and subtract it from the original. Yet for our purpose another approach have proved to be more suited. This approach is based on the a priori information of the structures considered, and utilises this information when construction the artificial background image.

As described in the beginning of this chapter, the present work is focused

on 2 cases : vesicles and tethers. A filtering that favours the straight, thin lines of a tether will not provide a good filtering of the circular vesicles with their bending, snake-like domain structures. Thus different filtering have to be invoked, and the solution to this have proved to be the choice of different structuring element, which will be introduced in the following.

Structuring elements

Structuring elements are chosen for the generation of the artificial background images. In order to understand the role of the structuring element, one must recall that the image is to be considered as a matrix with rows and columns according to the number of pixels. The structuring element is now a smaller matrix representing a geometrical shape. This may for instance be a "square", a "line" or a "disk".

$$\text{averaging: } \begin{bmatrix} 1 & 1 & 1 \\ 1 & 1 & 1 \\ 1 & 1 & 1 \end{bmatrix}$$

Yet it is possible, by modifying this matrix, to extract different features from the images. for instance line structures

$$\text{line structure: } \begin{bmatrix} 0 & 0 & 1 \\ 0 & 1 & 0 \\ 1 & 0 & 0 \end{bmatrix}$$

or disk like shapes

$$\text{disk structure: } \begin{bmatrix} 0 & 0 & 0 & 1 & 0 & 0 & 0 \\ 0 & 1 & 1 & 1 & 1 & 1 & 0 \\ 0 & 1 & 1 & 1 & 1 & 1 & 0 \\ 1 & 1 & 1 & 1 & 1 & 1 & 1 \\ 0 & 1 & 1 & 1 & 1 & 1 & 1 \\ 0 & 1 & 1 & 1 & 1 & 1 & 0 \\ 0 & 0 & 0 & 1 & 0 & 0 & 0 \end{bmatrix}$$

These matrices are called structuring elements, and their role in the filtering of images will be described below.

Morphological operations

Morphological operations on images are utilising the structuring elements to provide modified versions of the input images. The structure of the structuring element determine which geometrical elements of the original image that

will be emphasised. This allows for the constructing of artificial background images mentioned in section 4.1.2.

Now let X denote the pixel matrix of the image, and B the matrix representing the structuring element. Operations used in the present work are following:

Dilation:

$$X \oplus B = \left\{ p \in \varepsilon^2 : p = x + b, x \in X, b \in B \right\} \tag{4.1}$$

Erosion:

$$X \ominus B = \left\{ p \in \varepsilon^2 : p + b \in X, \forall b \in B \right\} \tag{4.2}$$

Opening:

$$X \circ B = (X \ominus B) \oplus B \tag{4.3}$$

Closing:

$$X \bullet B = (X \oplus B) \ominus B \tag{4.4}$$

For a visual interpretation of this, consider the "image" in figure 4.2. The image is a 10 x 10 matrix, consisting of 1's and 0's. Now performing the four above operations with a line or a disk element, given by

$$\text{line structure:} \begin{bmatrix} 0 & 0 & 1 \\ 0 & 1 & 0 \\ 1 & 0 & 0 \end{bmatrix}$$

$$\text{"disk":} \begin{bmatrix} 0 & 1 & 0 \\ 1 & 1 & 1 \\ 0 & 1 & 0 \end{bmatrix}$$

The results of applying these two 3 x 3 matrices as structuring elements on the picture in figure 4.2 are as displayed in figures 4.1.2-4.6 and 4.7-4.10, respectively. It is seen that the different structural elements preserves, enhances and suppresses different characteristics of the original image in figure 4.2.

Image histograms

The image histogram is the histogram of the pixelvalues of the image. By changing the distribution one may enhance the image. In the latter, two methods are used: image adjustment and equalisation of the image.
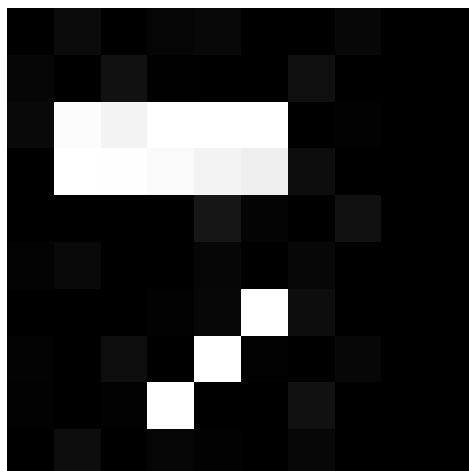
Figure 4.2: *Image consisting of 10 x 10 pixels of 1's and 0's.*

image adjustment adjust the intensity values of an image I such that 1% of the data saturated at low and high intensities of I. This increases the contrast of the output image J.

histogram equalisation enhances the contrast of images by transforming the values in an intensity image, or the values in the colormap of an indexed image, so that the histogram of the output image approximately matches a specified histogram.

The examples of performing these operations on vesicle pictures are displayed in figure 4.1.2.

4.1.3 Flow diagram of the image analysis

As mentioned in the beginning of this section, the two configurations, tethers and vesicles, demands different approaches as a consequence of the geometry of both the object and the domains. Yet some steps goes for both: In order to quantify the domains, one has to come from the grayscale images to a binary presentation, as we want to divide the lipid components into two categories : liquid or fluid. The grayscale images are stored as matrices with numbers in the range 0-250. Thus, one might expect that a simple thresholding would provide a proper classification of pixels as being either "gel" or "fluid". As gel domains appear dark, also background areas, i.e. areas without lipid, will appear dark. But since the illumination differs within each image as a

Figure 4.3: *Dilation of figure 4.2 using line element*

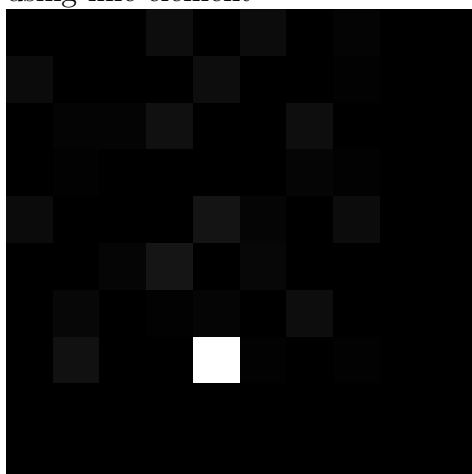Figure 4.5: *Opening of figure 4.2 using line element*

Figure 4.4: *Erosion of figure 4.2 using line element*

Figure 4.6: *Closing of figure 4.2 using line element*
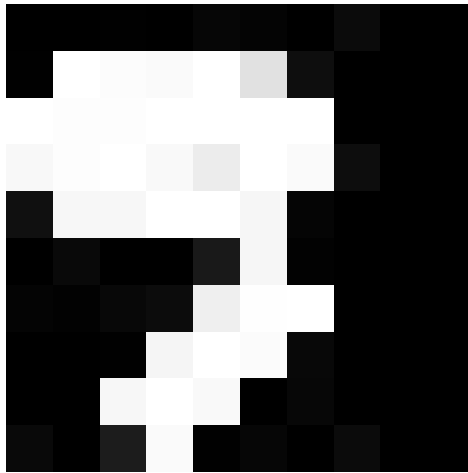
Figure 4.7: *Dilation of figure 4.2using disk element*

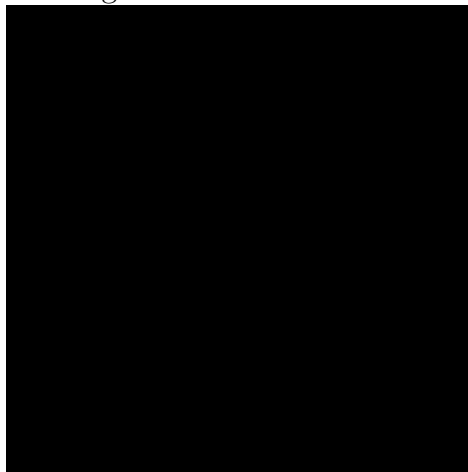Figure 4.9: *Opening of figure 4.2 using disk element*

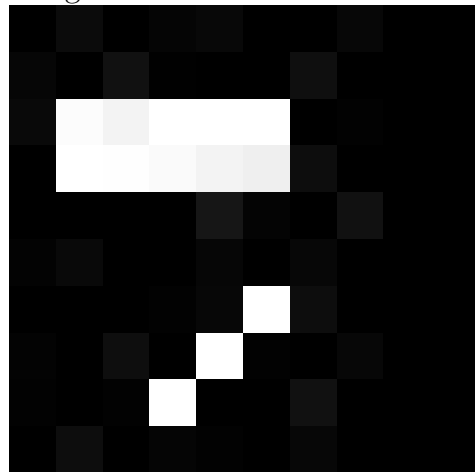Figure 4.8: *Erosion of figure 4.2 using disk element*

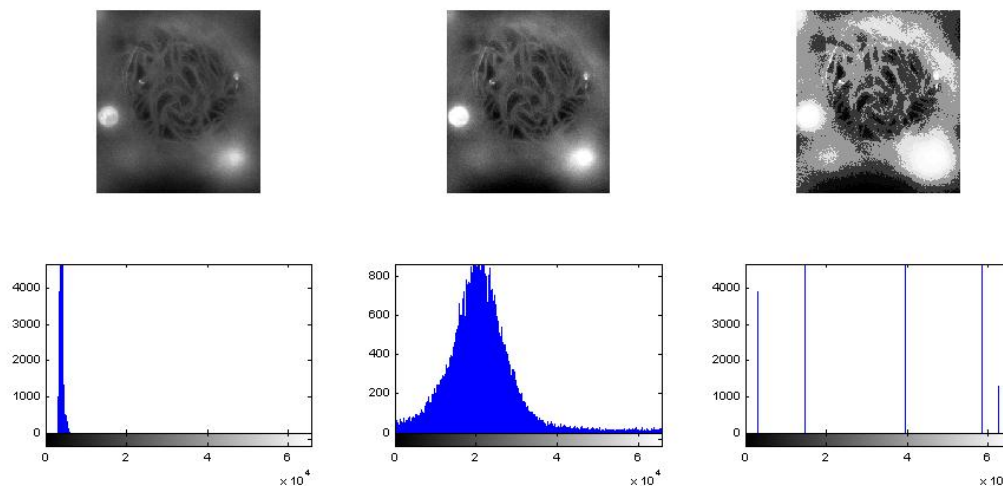Figure 4.10: *Closing of figure 4.2 using disk element*

Figure 4.11: *Image histogram - **Left** The original image, **Middle** Image with adjusted values,**Right** Image with an equalised histogram*

consequence of light scattering and clustering of lipid and dye, this is not the case. Thus a simple thresholding do not provide a reasonable sectioning.

An outline of the steps of the image processing is given in figure 4.12. One of the crucial aspects of image processing is that any filtering causes a change in the image properties, and may thus change the information which can be extracted from the image. I.e. a blurring of the image causes a blurring of the domains, causing some parts to grow, and some parts to shrink. It is thus a matter of judgement wether a given image processing approach is valid or not. The ultaimate goal is to build a processing routine which implements the knowledge an "eye" of the experienced experimentalist.

4.2 Analysis of fractional composition of the vesicles

The vesicle pictures are first filtered by creating a "background", and subtracting this form the picture. This background is generated as a blurring using a circular filter. There after the image is adjusted and converted to black and white using Matlab. See fig. 4.13., for an example.

Once the vesicle pictures have been converted to binary, the binary pictures are analysed using Matlab. After filtering of the image into a black/white
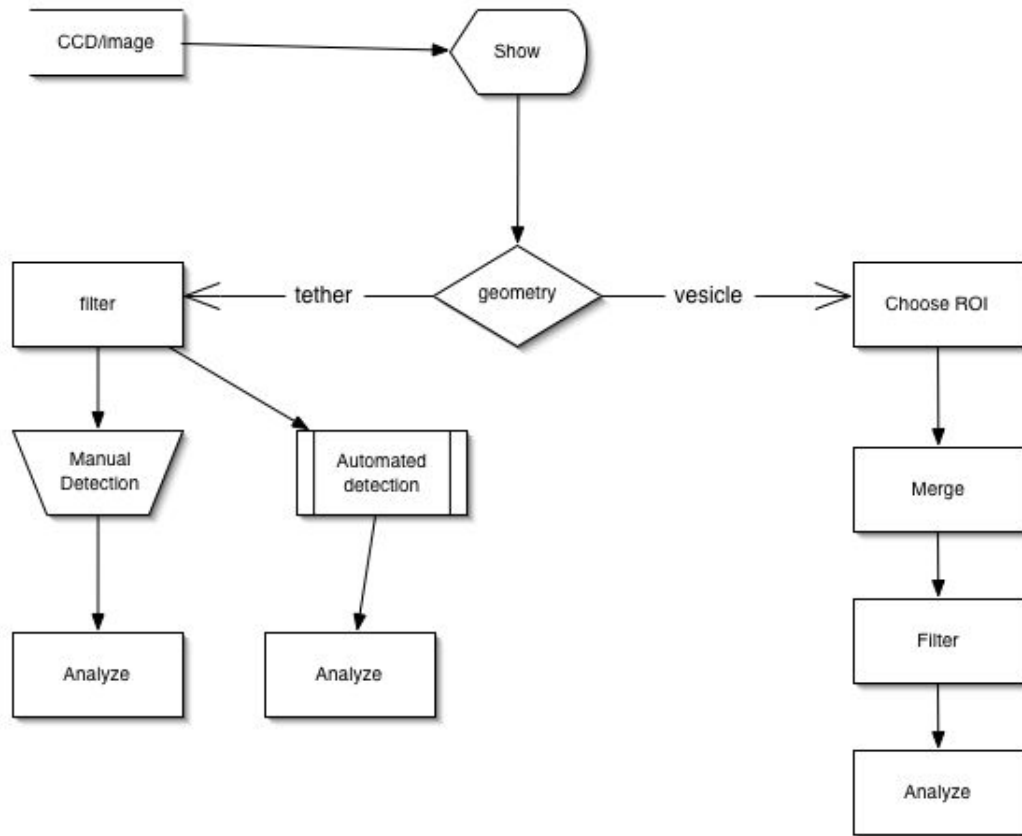
Figure 4.12: *Flow diagram for image processing. Depending on object type the proper processing is determined*
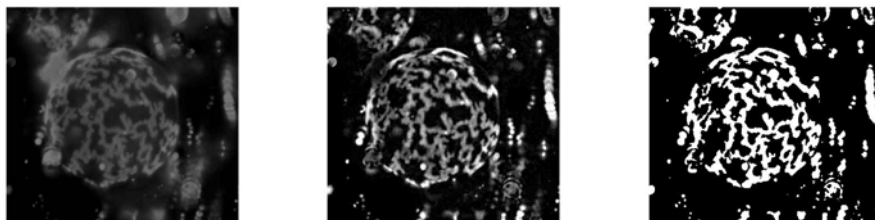
Figure 4.13: *Picture obtained by merging of stacks. The* **left** *shows the picture, the* **middle** *the picture with the background subtracted, and the* **right** *a black and white representation*
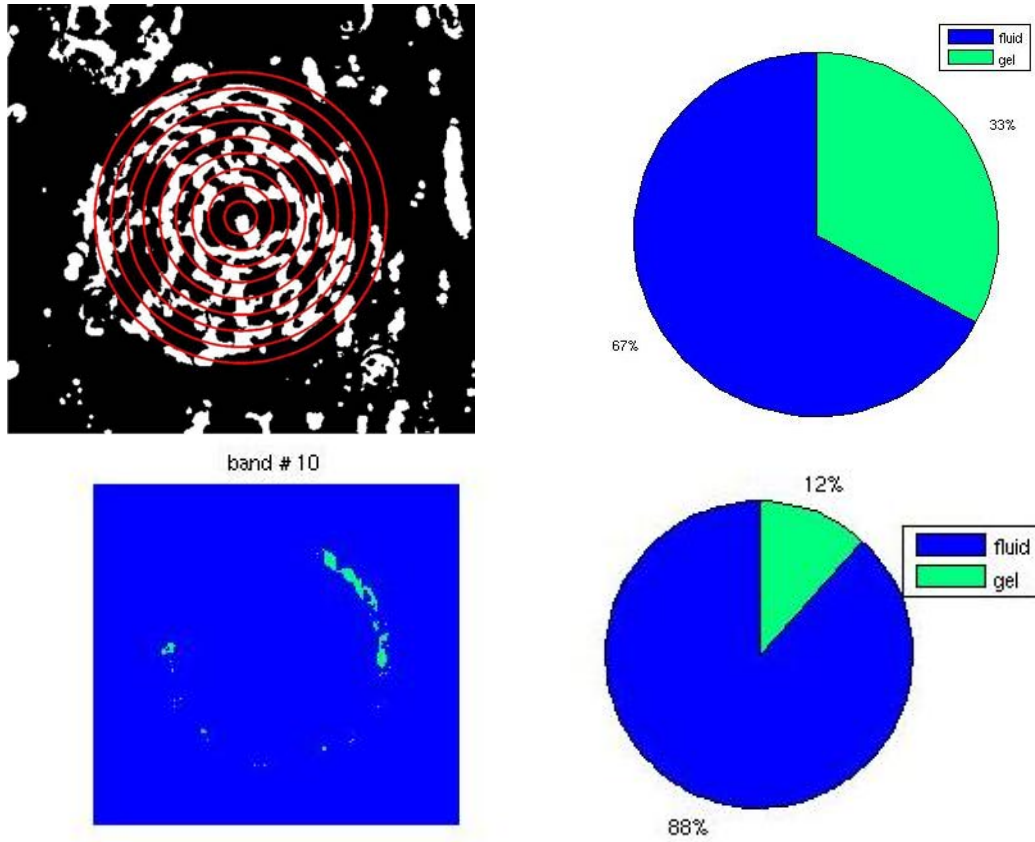
Figure 4.14: *Analysis of the fractional composition of a vesicle.* **Upper row** *shows the binary vesicle image, as well as the fractional gel-fluid comsition of the total vesicle.* **Lower row** *shows a single band of the vesicle, and the fractional composition analysis of this single band.*

presentation, the vesicles are analysed by specifying the centre and border of the vesicle. The area is now divided into a number of circular regions, fig.4.14 . In each of these regions the fractional composition of gel and fluid lipids are calculated by counting the number of black and white pixels. As this is done using a flat projection of a 3D object, one has to do a recalculation in order to get the real composition. This is done by assuming the vesicles to be spherical (or half-spherical) objects.

For each circular band, the area is

$$A_i^{circular} = \pi \cdot (r_i^2 - r_{i-1}^2). \tag{4.5}$$

The area of a cap of a sphere is given by

$$A^{cap} = 2 \cdot \pi \cdot R \cdot h, \tag{4.6}$$

and dividing the halfsphere into bands one finds for each half sphere band the area

$$A_i^{spheric} = 2 \cdot \pi \cdot R \cdot (h_i - h_{i-1}). \tag{4.7}$$

The height of the cap is

$$h_i = R - x_i = R - \sqrt{R^2 - r_i^2}. \tag{4.8}$$

Using the assumption that the vesicle is a half sphere, each vesicle is divided into i bands, and the number of gel and fluid pixels are calculated for each band. Applying the equations 4.5-4.8 to the number of bands gives a conversion factor

$$\gamma^{area} = \frac{\text{Area of half spere band}}{\text{Area of circular band}} \tag{4.9}$$

which is used to calculate the distribution when it is projected from the disk to the half sphere. When summing over all bands, one finds

$$\sum_i A_i^{spheric} = 2 \cdot \sum_i A_i^{circular} = \sum_i \gamma_i^{area} \cdot A_i^{circular} \tag{4.10}$$

For i $\rightarrow \infty$ one finds

$$\frac{\sum_i A_i^{spheric}}{\sum_i A_i^{circular}} = 2 \tag{4.11}$$

In the gel/fluid Matlab program, this is ensured by accepting only values 2±0.2.

Dye exclusion

When converting to a binary image, one must take special precautions in the case in which dye exclusion ins observed. The areas that show dye exclusion yield low pixel values, and will thus be regarded as "fluid". Yet this seems not to be the case. In the analysis routine one may manually mark areas showing dye exclusion, in order to extract this information from the image.

4.3 Detection and analysis of tethers

The tethers have been analysed using two different approaches. One using manual detection somewhat similar to that of vesicles, and another using automated detection. Analysis of the tethers requires a slightly more sophisticated approach than that of the vesicles. The tethers appear as thin and elongated structures compared to the rest of the object in an image. Further more the tethers show phase separation causing them to be only partially visible in the microscope as the dye favours the gel phase.

Automatic detection of lipid tethers seem to have been described previously only very recently in a paper by Hodneland et al. concerning automatic detection of tethers connecting vesicles [11]. The paper present a method for detecting tethers in 3D images stacks. The approach of [11] is quite time consuming (20min. pr. stack). In the following, it is shown, that for our problem, only 2D analysis is necessary. Furthermore, in the paper by Hodneland, the sample is described by two channels, one presenting the "image", and one channel only the interior of the vesicles. This provides a means to extract information of the tethers by removing the vesicles. This is not possible in our setup, and therefore the removal of vesicles have to bee accomplished by inventing another approach. Last but not least, our task is complicated by the fact that we do not see the entire tether in the image, but only the liquid parts, i.e. the domains the dye favours.

Tethers have in this work been detected by Hough transformation using a build in function of Matlab. Prior to this transformation the image are enhanced and converted from grayscale to black and white, as the Hough transform requires a binary input. For most purposes described in the literature, ex. [27], the Hough transformation is applied to a black/white image obtained by edge detection. Yet I have found this method to be less appropriate for the task encountered in the detection of tethers. Edge detection causes the two sides of the tether to be presented in the binary image, giving rise to too many lines being detected by the Hough transformation, as one tether segment now yields two long side lines. This is a problem that might be solved by blurring and filling the image after the edge detection. Yet this have not been implemented in this work.

4.3.1 The Hough transformation

The Hough transform is an algorithm widely used in computer vision for detection of lines in noisy images. It was first described by Hough[12] where it

Figure 4.15: *Image for test of the Hough transformation. It consist of 35 points in a 100 x 100 pixel image.*

was implemented as a tool for detection of particle tracks in bubble chambers.

Going from image to the Hough Domain   As a simple example, consider a plane in which a number of points are detected, see fig. 4.15.

Each point $i(x, y)$ is now described by a vector $\vec{\rho_i}$ of length ρ from the origin of the plane O(0,0) to the point i, through the angle θ with the x-axis,

$$\rho_i = x\cos(\theta_i) + y\sin(\theta_i) \tag{4.12}$$

Doing this for all points, the Hough transform accumulates a set of $(\rho_i, \theta i)$, i.e. sets of slope of the line along the vector, and its intersection with the y axis.

Consider the simple image in fig. 4.12 for an example of applying the Hough transformation. Out of the 35 particles in the image, the eye easily detects two straight lines consisting of 10 points each. Now through each of these points, a line spanning the image plane is drawn. It is rotated through the interval $\theta \in [-90°, 89°]$. For each bin of the size 1°, the number of points on the line, N_i is registered. Plotting the transformation will thus, for each particle in the image, give a curve consisting of the pairs (θ, ρ), with the point value N_i. The result is visualised in figure 4.16, and in figure 4.17 the extracted lines are superimposed on the original image.

Going from the Hough Domain to the image   The Hough transform on its own provides information of angle and intersection with the y-axis of
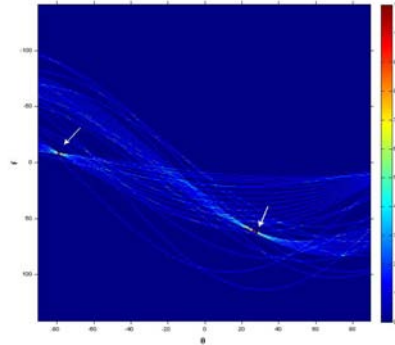
Figure 4.16: *Visualisation of the Hough domain of the image in figure 4.15. Each wave in the visualisation represents the rotation of a line about a point in the image of figure 4.15 about the angle θ, giving an intersection ρ with the y-axis. The colour of each point on the wave shows the number of point on that line. The minimum value of a point on one of the curves is 1, i.e. the line hits only the point about which it is rotated. The white arrows indicate the two maxima.*

any line in the image. But the Hough transform in itself do not yield information of how long the line segment is. As the exact length and placement of each line element is often an information of interest, as is the case in our particular problem of tether detection, one has do some additional mathematical operations. That is, one have to impose the information of the peaks in the Hough transform, presented in the form (ρ, θ), on the original image, and there by detect points constituting lines.

4.3.2 The Hough transformation using Matlab

The theory of line detection using the Hough transform was implemented using Matlab. The Matlab functions used will be described briefly in the following.

hough The basic hough transformation function. It returns a Hough transform matrix H of two dimension, $\theta x \rho$. The θ-values denotes the angle, and lies in the range [-90:89]. R denotes the intersection of the line perpendicular to $\vec{\rho_i}$ with the y-axis, and lies in the range [-l:l] where l is the diagonal of the image. The resolution of θ and R bins can be specified, and affects the dimensions of θ and ρ.
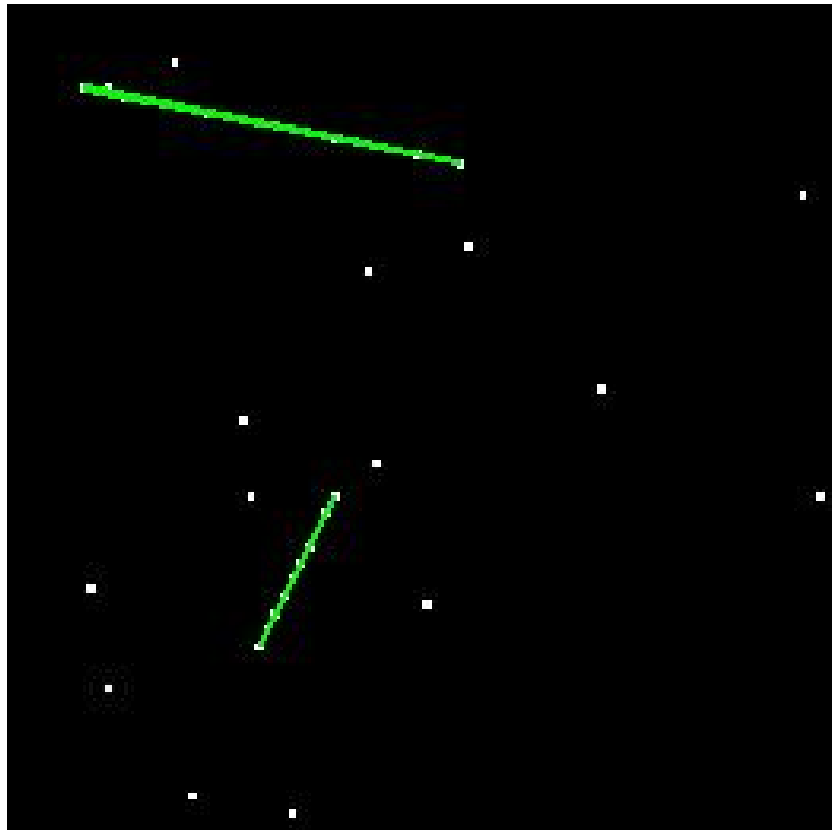
Figure 4.17: *Two lines detected in figure 4.15 by Hough Transformation.*

houghpeaks detection of peaks in the hough domain. A threshold for the definition of a peak, i.e. the lowest amount of particles that can constitute a line can be specified.

houghlines detection of lines in the image, based on combining information of the hough transformation with the original image. This command overcomes the problem of the image spanning lines detected by the Hough transform. The endpoints of line segments are provided by the command. It is possible to specify constraints of minimum line length and maximum gaps within one line segment. That is, lines that are not continuous can be detected if wanted.

Implementing th Hough transformation in Matlab is relatively simple, as may bee seen in Appendix C. The most problematic part is to perform a good filtering for the extraction of a black and white image, showing only the structures of interest, in the present case the line element. The best results have been obtained by choosing a line structuring element with an angle depending on the direction of the tethers. This means that the best filtering is obtained when the tethers are aligned, which is often the case as a consequence of the flows in the chamber.

4.3.3 Demonstration of the tether detection

An example of the use of the developed program are given in figures 4.18 and 4.19. The program shows a detection efficiency which is fair, but with room for improvement. It was developed for the analysis of images showing a large number of tethers, at different temperatures. Unfortunately the experimental part of this thesis did not yield sufficient of such pictures. Those pictures which showed tethers have there fore been analysed using a manual detection.
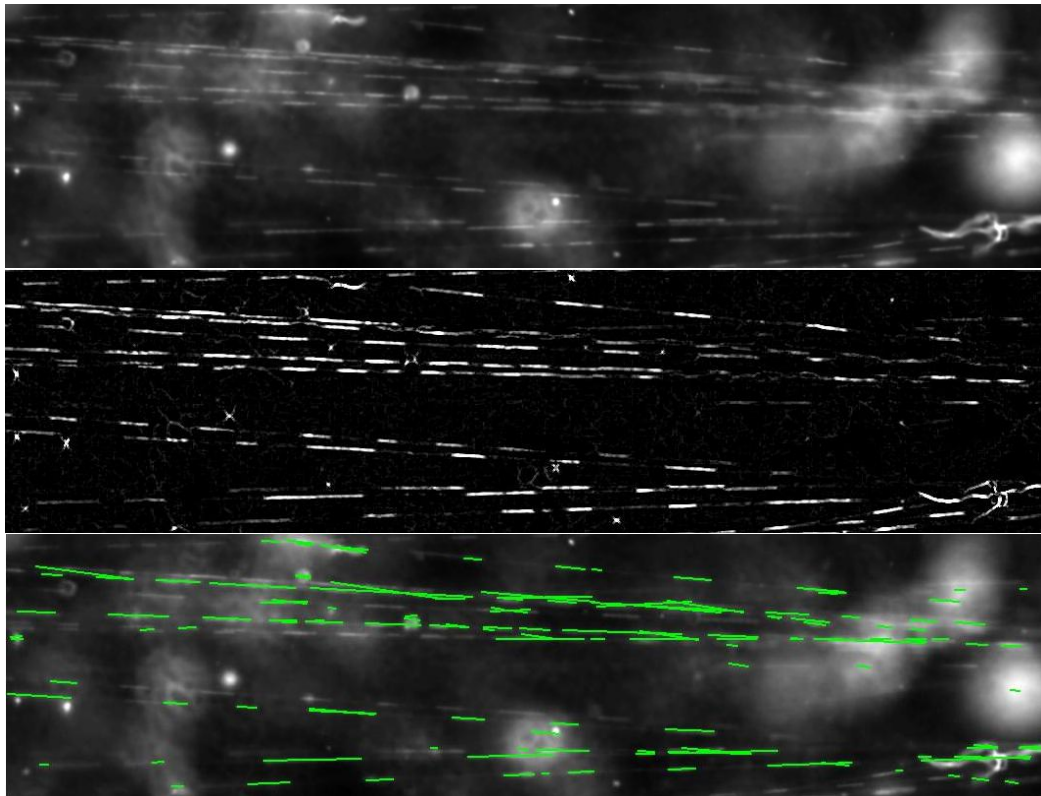
Figure 4.18: *Tethers at appr. 10°C.* **Top**: *CCD picture.* **Middle**: *Filtered picture, Matlab.* **Bottom**: *Domain lines detected using Hough tramsformation, Matlab*
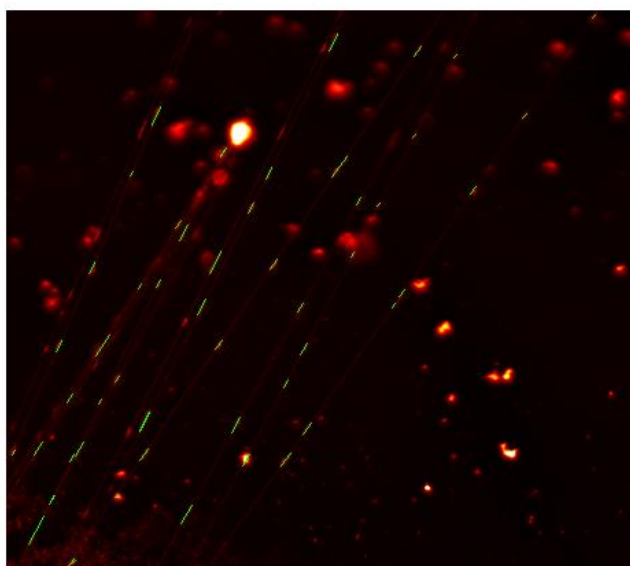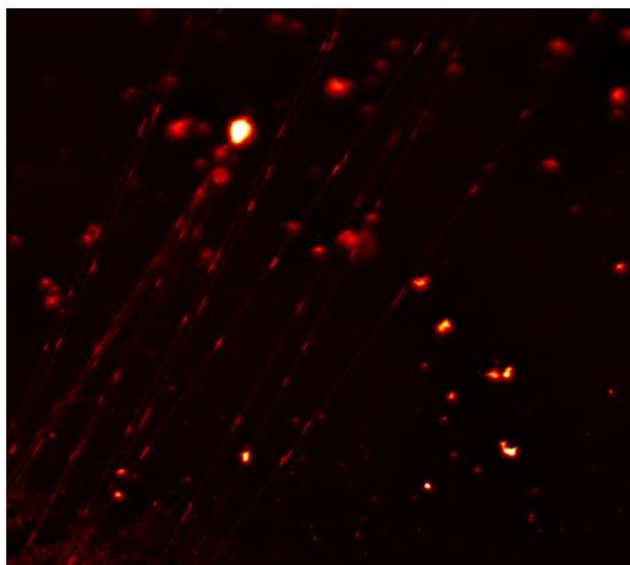
Figure 4.19: *Tethers at appr. 10° C*

Chapter 5

Results

In this chapter, the results obtained during the experimental work will be presented. The first section will describe and analyse the results obtained from calorimetric measurement. There after the data obtained from microscopy will be presented and analysed, and finally compared to the information obtained by calorimetry.

5.1 Calorimetric measurements

The excess heat capacity of the different samples were measured using differential scanning calorimetry. Profiles for pure lipids and different lipid mixtures are found in fig. 5.1.

5.1.1 Lipid membranes

One obviously sees that the transition of a mixture is not only given by a superposition of the two pure lipids. That is, the calorimetric measurement yields the information that there is interaction between the lipid species.

5.1.2 Lipid membranes and dye DiI-C18

It has previously been demonstrated that Di-C_{18} in a DLPC:DPPC system has a preference for the gel phase [5]. In this section the focus will there fore be on Di-C_{18} in DMPC and 1:1 DMPC:DPPC systems. According to the theory of the Mattress model described in the Theory chapter, the insertion of Di-C_{18} , which has a chain length larger than that of the membrane lipids, should favour the gel state, thus lowering the transition temperature.
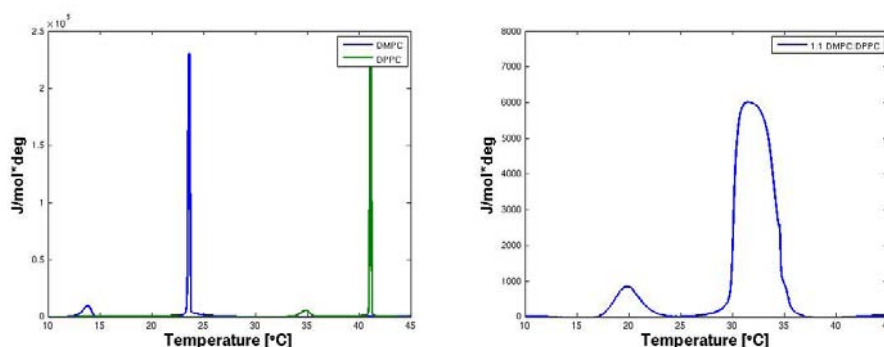
Figure 5.1: *Measured excess heat capacity curves. Pure DMPC, DPPC, and a 1:1 DMPC:DPPC sample.*

Examining the influence on the heat capacity of a single component DMPC membrane, figure 5.2, tells that the transition temperature of the main transition is slightly lowered. In addition to that the pre transition is depressed by the insertion of Di-C$_{18}$. The effect on the two-component 1:1 DMPC:DPPC system is less profound, as seen in figure 5.3. Yet taken the CCD pictures into account, it is most likely that the Di-C$_{18}$ has a preference for the gel phase.

5.2   Vesicles

As described in the Materials Section vesicles are formed at a temperature well above the phase transition. An example of vesicles was presented in given in the introductory chapter. One sees that not only GUV are formed, but that smaller vesicle may form inside larger. The vesicles range in the order 10-100μm, and are thus comparable to living cells. The vesicles differ in shape but show with few exceptions a close-to circular shape of the ground section.

An interesting phenomenon is the occurrence of moving domains which may be observed in the upper temperature range of the phase transition. This phenomenon has not been investigated in detail, but the interested reader may download movies of moving domains on the webpage of this thesis [1]

---

[1]www.nbi.dk/∼lundgard/thesis

Figure 5.2: *Measured excess heat capacity curves for DMPC with 1 mol %
dye .*
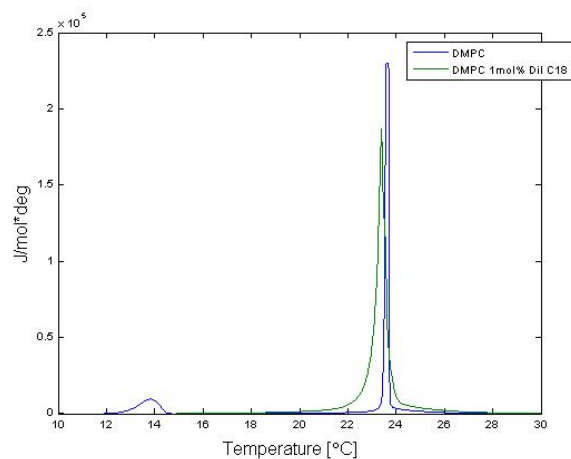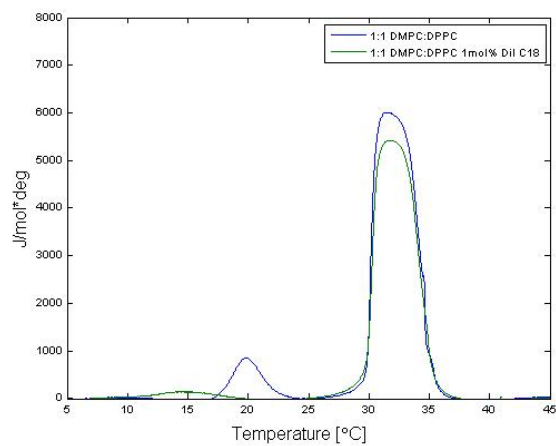

Figure 5.3: *Measured excess heat capacity curves for DMPC and 1:1
DMPC:DPPC with 1 mol % dye.*
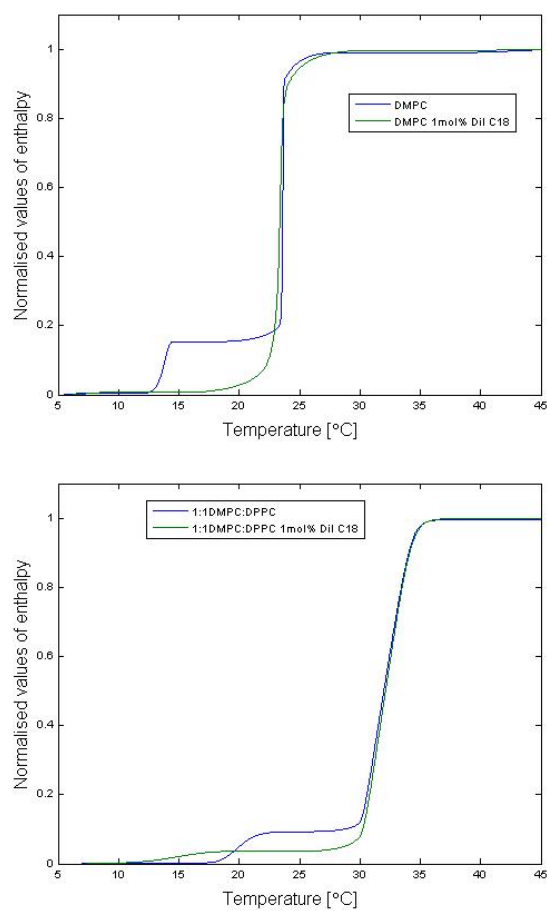
Figure 5.4: *Normalised phase transition enthalpy curves for DMPC and 1:1 DMPC:DPPC with 1 mol % dye.*
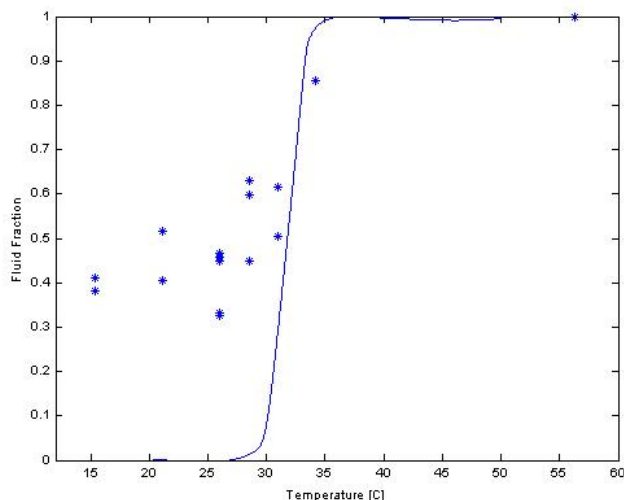
Figure 5.5: *Gel and fluid fraction of vesicles as a function of temperature. The sample is 1:1 DMPC:DPPC*

5.2.1 Gel and fluid fraction of vesicle as a function of temperature

As described in the Theory Section, and in the motivation of this thesis, it is of interest to investigate the gel/fluid fraction as a function of temperature, and compare this with the accumulated enthalpy curve derived from calorimetric measurements. In figure 5.5 results are presented from vesicles made from 1:1 DMPC:DPPC. Apparently all-gel vesicles are not observed. Yet this is most likely to be a consequence of the dye being "locked" in the gel domain. It is observed that the vesicles crumple when cooled as showed in figure 5.9. A way to overcome this effect may be to **a** use another dye, or **b** use another experimental approach.

5.2.2 Exclusion of dye

Exclusion of dye from circular/hexagonal areas has been observed, example figure 5.6. It is a phenomenon that is reported in the literature, but an explanation of the origin has not yet been given. The experimental procedure followed in the present work allows for continual study, and it is interesting to see, that gel domains form from the areas of dye exclusions, see figure 5.7.

The distribution of the size of the dye exclusions seems to be of a limited
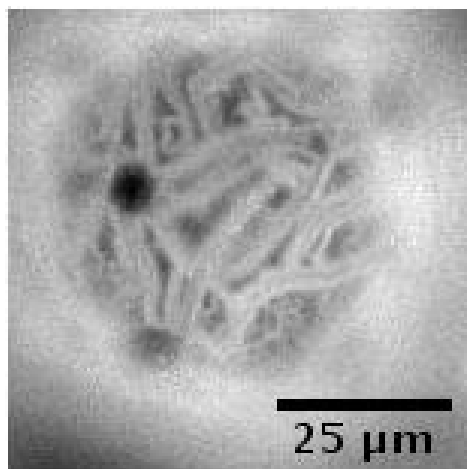
Figure 5.6: *Vesicle at approximately 23°C , 1:1 DMPC:DPPC. The domains separation is profound, as well as two nearly circular areas of dye exclusion*
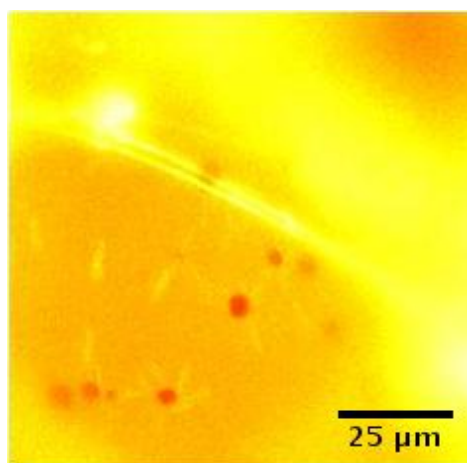
Figure 5.7:   Vesicles showing beginning phase separation around areas of dye exclusion, 1:1 DMPC:DPPC, 34 °C

area, see figure 5.8.

5.2.3   Stability of vesicles

The vesicles can maintain their shape over several days. If cooled in to the all-gel temperature range, they crumple up as may be seen in figure 5.9, and larger vesicles are likely to be destructed by the crumpling. The vesicles not destructed by the shape deformation caused by cooling resume spherical structure upon heating.

5.3   Tethers

Spontaneous formation of tethers was observed in the course of vesicle formation. It is a phenomenon often observed in vesicle studies, and is often regarded as uninteresting, or as disturbing obstacles. In this study however, the formation and properties of these tethers have been investigated. Some studies, e.g.. [1], [22], has addressed the topic of selforganised lipid tethers, but not with regard to phase transition.
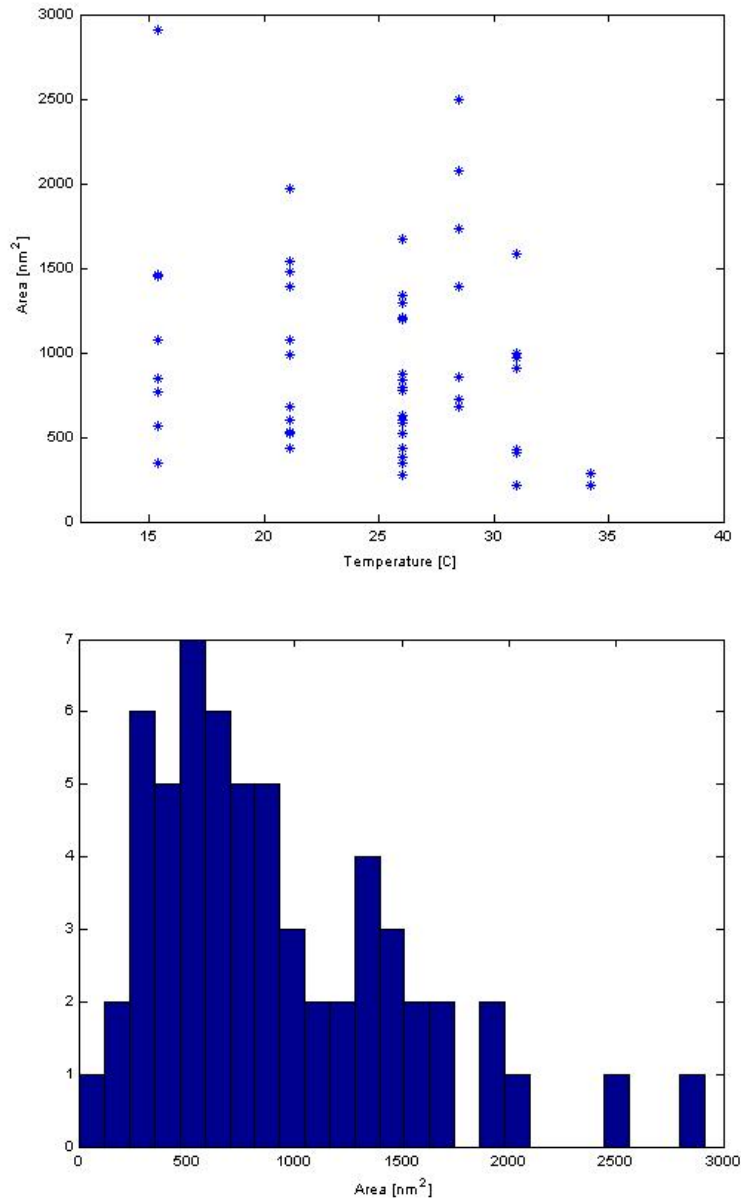
Figure 5.8: **Top:** *Size of dye exclusions as a function of temperature.* **Bottom:** *Size distribution of dye exclusions of 1:1 DMPC:DPPC independent of temperature*
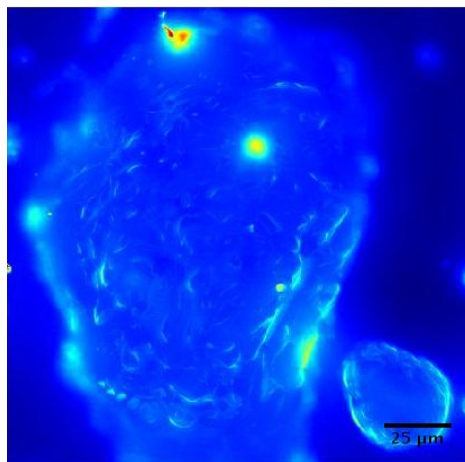
Figure 5.9: *Vesicle at approximately 15°C , 1:1 DMPC:DPPC. The vesicle shows a crumpled surface as a response to the cooling in to the all gel domain. At may regain its spherical structure upon heating.*

5.3.1   Process of Tether formation

Tethers were found to form spontaneously in the course of vesicle formation using the procedure described in the Materials chapter. Furthermore, they were observed to grow spontaneously out of the lipid layer as a consequence of the flows in the chamber. That is, vesicles are being moved along with the flows in the chamber, dragging long 'tails" of tethers out of the lipid layer on the ITO.

Areas with tethers often divide into two groups. One in which the tethers are highly aligned, and those strings are then most likely formed as a consequence of flows in the chamber. The other tendency is that they are in several directions. In these cases the tethers are most likely formed as a consequence of brownian motion, pulling vesicles and tethers in random directions.

5.3.2   Domain formation on tethers

As the vesicles show domain formation and separation, so do the tethers, see figures 5.10 and 5.11. It has not been possible to study the temperature dependence of the domains in the tethers in detail, but still Sime conclusions can be made. The domain formation is reversible, i.e. providing that the tethers are not disturbed or destroyed one may induce domain forma-
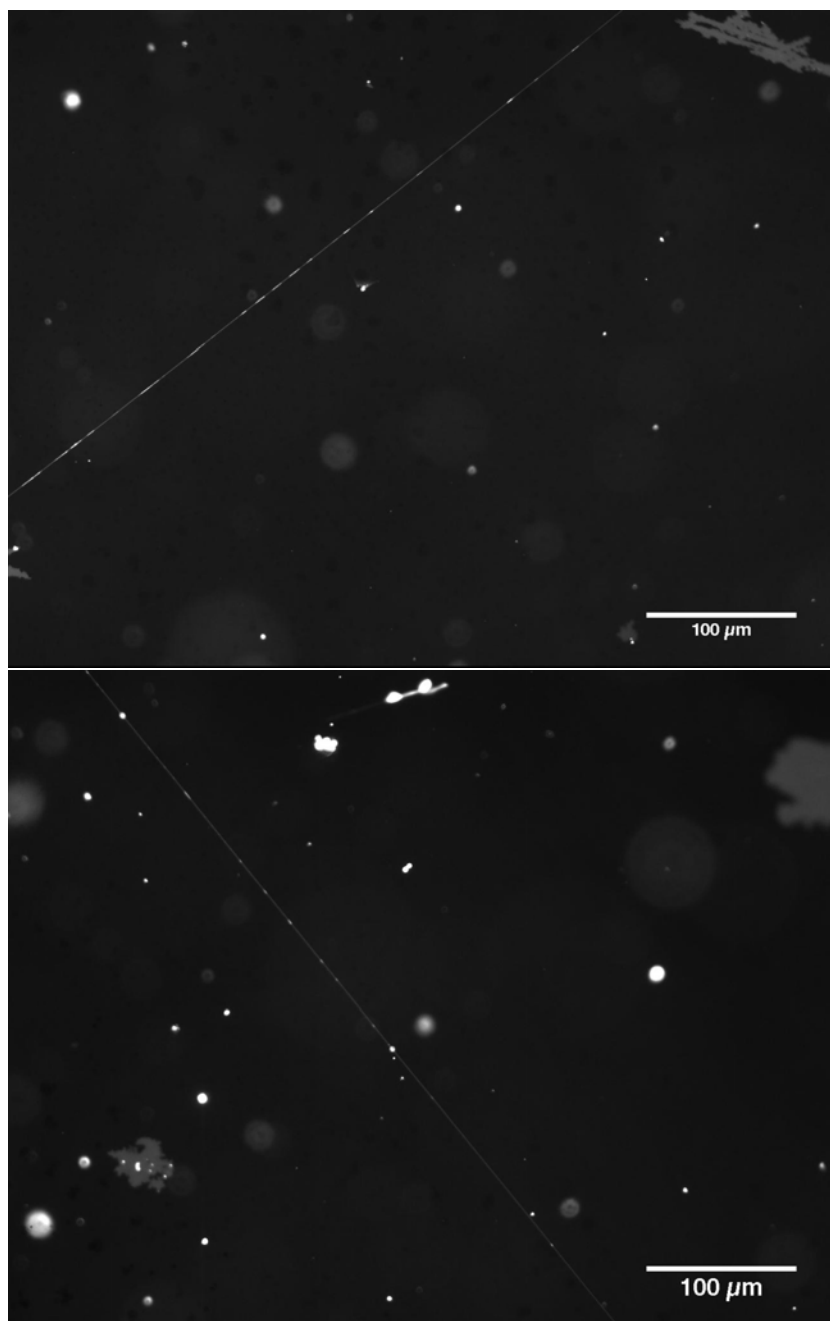
Figure 5.10: *Examples of a tethers showing domain separation. Sample composition is 6:4 DLPC:DPPC, at 20°C*
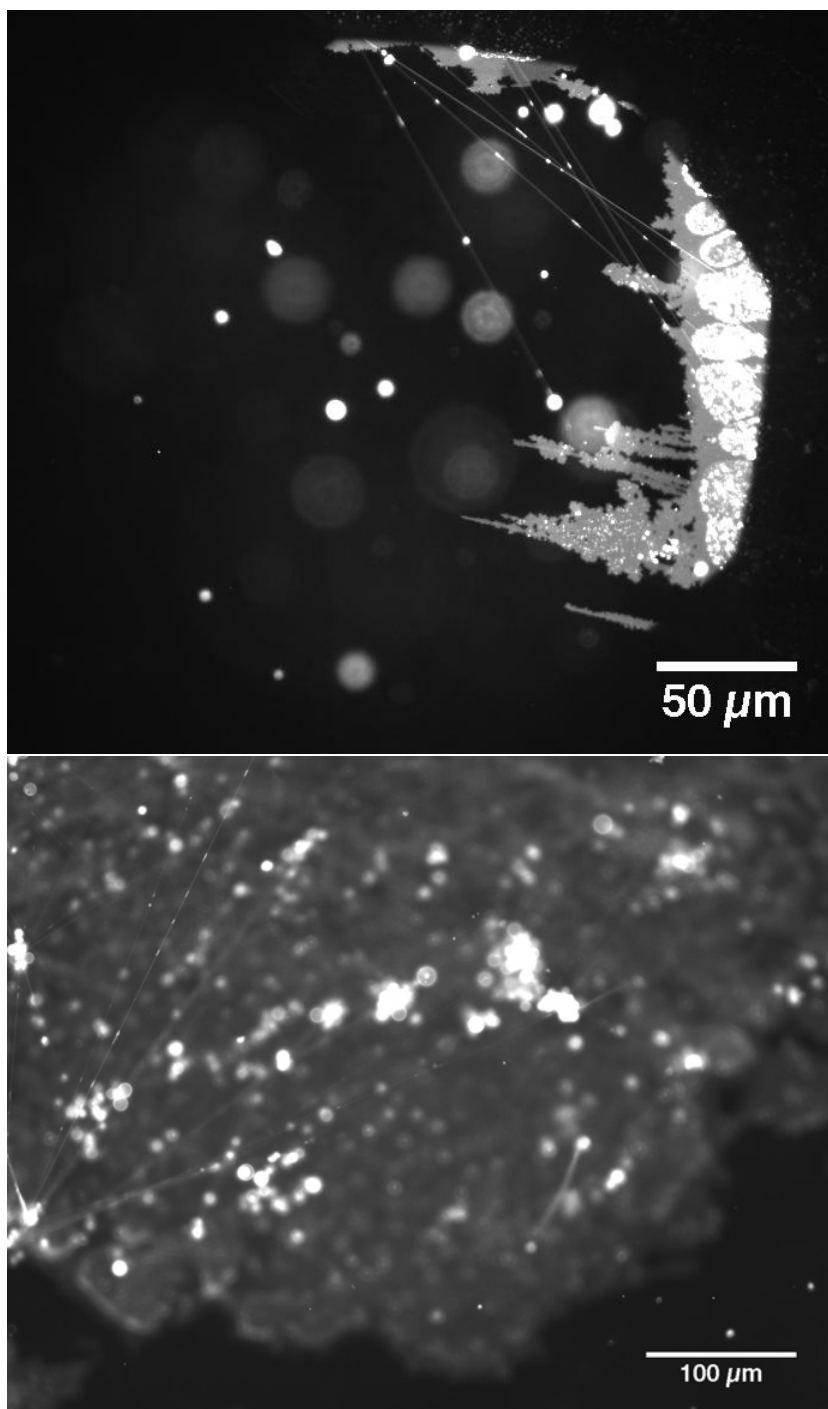
Figure 5.11: *Examples of a tethers showing domain separation. Sample composition is 6:4 DLPC:DPPC, at 20°C*
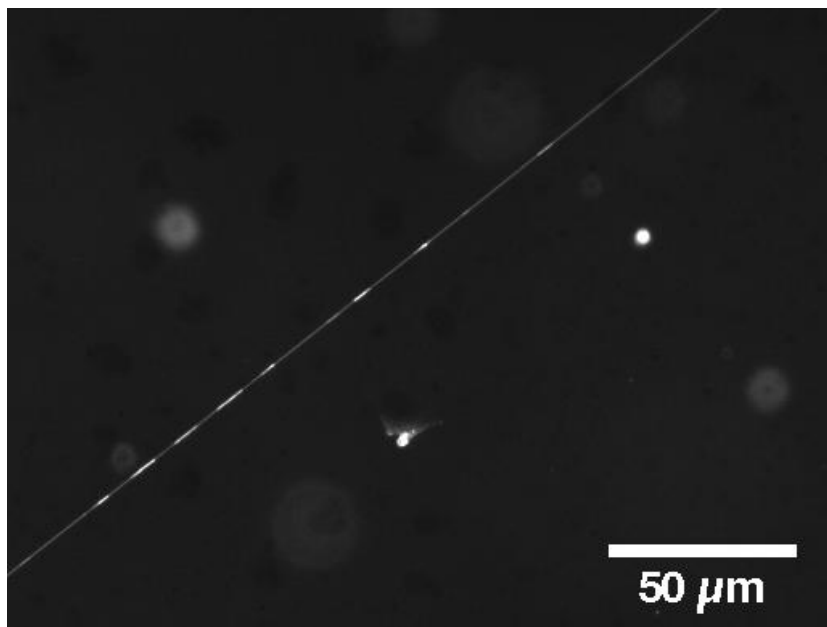
Figure 5.12: *Example of a tether showing domain separation. Sample composition is 6:4 DLPC:DPPC, at 20°C .*

tion by cooling, and restore the all fluid tether by heating. The domains seem in some cases to distribute with some periodicity on the tethers. Fig. 5.13 present autocorrelation spectre of the gel/fluid profiles of the tethers. Without going into details on autocorrelation, it should just be noted that peaks indicate periodicity. As seen, this is the case for some, but not for all tethers. There seem to be, if not periodicity, then at least an upper limit to the sizes of the gel and fluid domains in the tethers. This may indicate that there is a finite upper/lower limit on the domain size, determined by the lipid composition of the tethers, and by the surface and line tension of the domains.

Another property worth considering is impact of gel/fluid phase on the diameter of the tether. This is difficult to measure, given the resolution of the camera, see fig. 5.12, but it seems clear that the diameter is increased in the gel phase. This is in good agreement with the bilayer thickening as the fatty acid chains become straight and aligned.
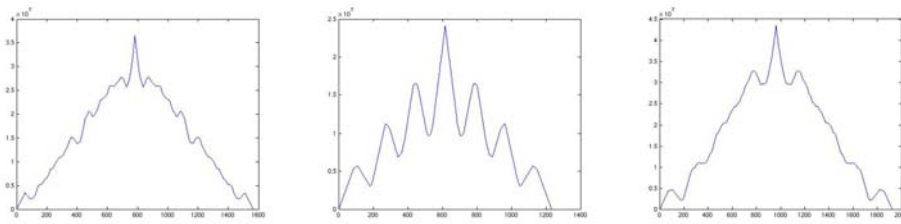
Figure 5.13: *Example of autocorrelation of tether profiles*

Chapter 6

Conclusion

In this section an overview of the results and innsights obtained during the work will be presented and compared to relevant examples from the literature. Second, a number of suggestions for improvements of the methods and further work in the field will be proposed.

6.1 Discusson of results

It has been shown that phase separation in lipid vesicles can be studied using simple fluorescence microscopy, and that an information content comparable to that of confocal microscopy can be obtained. Further more the use of the simple procedure allows for real time studies of domain formation.

Phase separation in spontaneously formated lipid tethers has been observed. It has not been possible to measurements over a temperature range comparable to those done on vesicles, but still some conclusions can be drawn from the tether study. Two findings shall be pointed out here:

- Domains form on the tethers when cooled from the fluid to the gel phase.

- The process of domain formation is reversible in tethers as well as in vesicles as the domains disappear again when heated above the phase transition temperature.

- Tethers may form spontaneously from a lipid bilayer exposed to flows, and may have a high degree of interconnectivity, both in the form of tether-tether connections and tether-vesicle connections

Other studies have shown that it is possible to obtain a forced phase separation in lipid membrane tubes[2], [23] by stretching, yet the occurrence of phase separation in systems like the ones studied in the present work has to our knowledge not been reported previously. Studies by Mahajan et al. [20] has reported an effect of the chirality if the lipids on the tethers. The thickening of the tethers upon cooling may be compared to measurements on the phase transition in nerves, by Tasaki [30]. This is of interest as the tethers may be seen as simplified models of nerves.

6.2   Outlook

Based on the experiences gained during the work on this thesis, it stands clear that the phase behaviour of lipid tethers would be interesting to study closer. A number of interesting topics could and should be addressed from an experimental approach. Three interesting projects on tethers could be

- A study of the spontaneous tether formation. This could be enhanced by controlling the temperature gradients in the chamber, by connecting it to two different water baths. In this way, a constant temperature gradient in the chamber could be maintained. This would cause the tethers to be aligned with the flow, and might lower the tendency of floating objects to be caught in the lipid nets.

- A study of tethers using micromanipulators would allow for much better control of the tethers. In this way single tethers could be studied and manipulated. A project in collaboration with the Optical Tweezers Group at the Niels Bohr Institute might also yield interesting results in the field.

- In relation to the experiments using fluorescence microscopy, computerized methods for image analysis has been developed. While there is still room for improvement, the present study can provide the basis for further development. In the paper by Hodneland et. al [11], a success rate of 67% for the automated detection compared to that of a manual is reported. With the present experimentla setup only one image channel is available, where two are available in the setup of Hodneland. Further work on automaitng the image analysis from the experimental setup like the one used in the Membrane Biophysics Group would be of great practical use. Collaboration with for instance image analysis groups at the faculty or other universities could very like result in time-saving analysis procedures.

The combined development of a controlled way of producing many tethers, and refinement of the tether detection programs has a perspective of providing more insight in to the formation of domains on tethers. A number of mechanisms for producing phospholipidid tethers are documented in the literature, e.g. the use of microfluidic technology[19] and mechanical manipulation [15].

The phase separation in tethers is of special interest when regarded as a model system for nerves. In recent papers it has been proposed that function of channel proteins may to large degree depend on the surrounding lipids [18], [24]. The opening and closing of channel proteins are widely recognised as the mechanisms producing action potentials in nerves. In the light of these findings, the possibility of domain formation in tethers is of interest, as the opening and closing of channel proteins is believed to be localised processes, travelling along the nerve with the action potential. Though not an established theory, the recently proposed Soliton Model [9], proposes a very different way of describing the action potential of nerves, namely as a propagating density wave, a soliton. The finding of domains on tethers is therefore of great interest in the light of this explanation of nerve pulses. If one could develop experiments in which the observed tether domains were observed to move, as it may be on vesicles, this would be a significant finding.

Appendix A

Protocol for image analysis

The analysis of the CCD images were done using tools developed using Matlab. While the underlying theory is described in the chapter on image analysis, this appendix will give a brief introduction to the practical implementation, procedure and graphical user interface.

When analysing an image sequence, the first steps are to

1. load the image sequence

2. determine the range of images of interest, i.e. the number of pictures taken during a vertical scan which should be taken in to account

3. perform a Z-projection of the images, i.e. mergin in the Z direction. A simple merging can be done using "merging.m".

After this pre processing steps, the image obtained by Z-projection can be loaded in to either the vesicle or tether detection programs.

A.1   Analysis of vesicles

Once the image is loaded in to the vesicle graphical user interface, figure A.1,it should be filtered to obtain a binary picture. This is done using a structuring element as described in the chapter on image analysis. Yet the size of this may have to be changed, depending on the size of domains. The user interface allows the user to decide when an appropriate filtering has been obtained. When the filtering is satisfying, the user may indicate centre and border of one or more vesicles, as well as centre and border of areas of dye exclusion, if any.
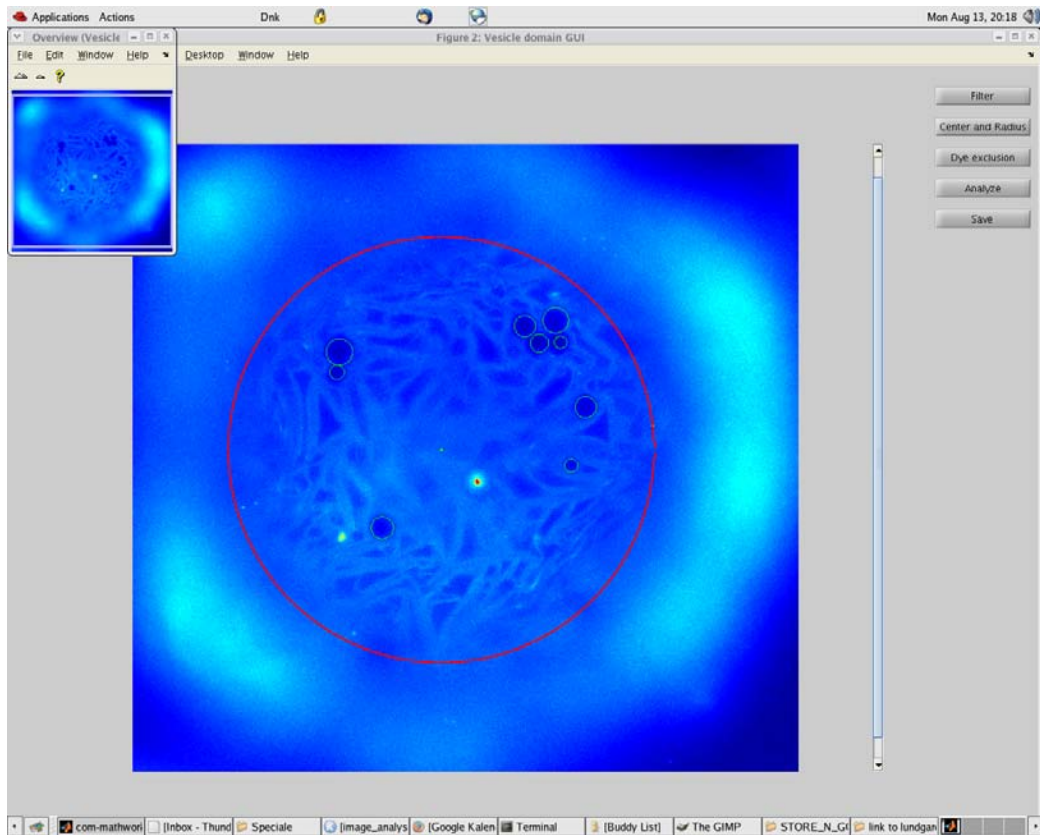
Figure A.1: Graphical user interface for vesicle analysis. Dye exclusion may be marked by green circles, and vesicles with red circles

After this the vesicles can be analysed, and the results stored in a .mat-file.

A.2 Analysis of tethers

The image is loaded in to the graphical user interface, figure A.2. The end points of the tether is specified, and there after the domains are specified. When all domains are detected, the tether may be analysed, and the result stored in a .mat-file.
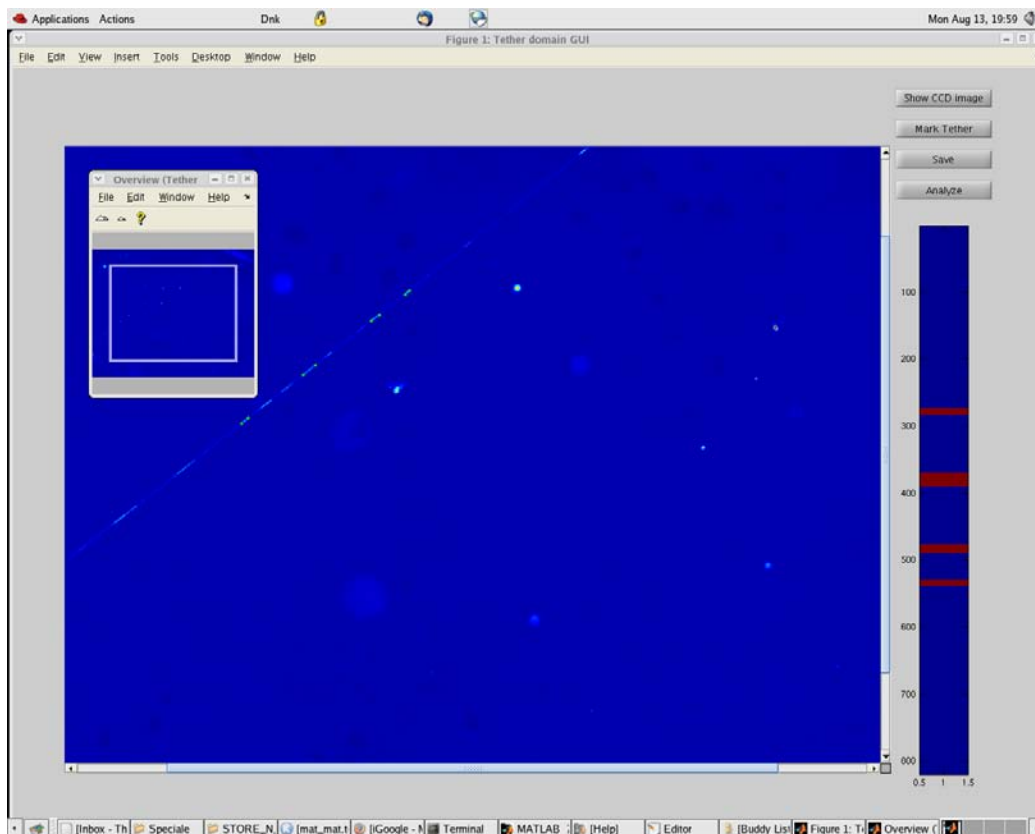
Figure A.2: *Graphical user interface for tether analysis. The end points of tether domains are marked with green dots. The tether profile is shown in the right side of the display, with the gel domains being red.*

Appendix B

Notes on electro formation procedure

The formation of vesicles is one of the crucial steps in the experimental work of this thesis. At times it may seem as if the succes is of the electro formation more or less random. Yet I choose to bellieve that this is not the case, and in the following a number of factors are listed that has proofed to be essential for a succesfull formation, along with a few tips and tricks for a succesfull electroformation of vesicles.

- a thourough cleaning of the thin ITO is required. Make sure that the ITO is as clean as possible, and bbserve that the lipid spreds nicely on the surface. If the lipid solution does not spread nicely on the ITO, one may as well try to clean the ITO and try again. Electroformation using an inhomogeneous lipid layer just wont work!

- Shield the electroformation chamber in order to avoid to much flow. It seems that this may make the formation of large GUV's more likely, as well as reduce the amount of freely swimmming lipid/dye clusters.

- The concentration of the lipid solution may play a role. Thin solutions may not provide lipids enough for the formaion of vesicles, and to high concentrations may lead to the formation of multilammellar vesicles, manking the phase separation impossible to detect with the microscope.

A frequently occurring problem was insufficient spreading of the solution on the ITO's. Even small impurities on the surface of the ITO may disturb the spreading. In these cases, a very thorough cleaning of the ITO's was carried out. The ITO's were cleaned in mucasol, ethanol and distilled water, all of these for up to 30min in an ultrasound waterbath.

Appendix C

Matlab functions

In the following the programs used for datanalysis of images will be described. The programs may be downloaded from www.nbi.dk/~lundgard/thesis.

C.1 Vesicle filtering and analysing

The program used for classification of gel and fluid domains in vesicles.

```
function vesicle_gui_scroll(I,temp)

 global BW filter_radius hFig;
filter_radius=10;
global VN current_data FRAC DEN VesicleDye AreaVesicle;
VN=0;    %vesicle number
DEN=0;   %Dye exclusion area number
global circx circy circy_comp centern centerm radius
global centerndye centermdye radiusdye circxdye circydye circy_compdye;
current_data=I;
AreaDye=0;


%--------Specify GUI layout---------------

scrsz = get(0,'ScreenSize');
   %  Create and then hide the GUI as it is being constructed.
   f = figure('Visible','off','Position',[1 scrsz(4) scrsz(3) scrsz(4)]);
   %  Construct the components.
   hFilter = uicontrol('Style','pushbutton','String','Filter',...
          'Position',[scrsz(3)*0.9,scrsz(4)*0.95,120,25],...
```

```
        'Callback',{@Filterbutton_Callback});

 hCenterRadius = uicontrol('Style','pushbutton', 'String','Center and Radi
        'Position',[scrsz(3)*0.9,scrsz(4)*0.95-40,120,25],...
        'Callback',{@CenterRadiusbutton_Callback});


hDyeExcl = uicontrol('Style','pushbutton', 'String','Dye exclusion',...
        'Position',[scrsz(3)*0.9,scrsz(4)*0.95-80,120,25],...
        'Callback',{@DyeExl_Callback});

hAnalyze = uicontrol('Style','pushbutton','String','Analyze',...
        'Position',[scrsz(3)*0.9,scrsz(4)*0.95-120,120,25],...
        'Callback',{@Analyzebutton_Callback});

hSave = uicontrol('Style','pushbutton','String','Save',...
        'Position',[scrsz(3)*0.9,scrsz(4)*0.95-160,120,25],...
        'Callback',{@Savebutton_Callback});

haCCD = axes('Units','Normalized','Position',[0.05 .1 .8 .8]);

%haFrac = axes( 'Units','Normalized','Position',[0.85 0.1 0.15 0.20]);

align([hCenterRadius,hSave, hAnalyze, hFilter, hDyeExcl],'Center','None');

% Initialize the GUI.
% Change units to normalized so components resize
% automatically.
set([f,haCCD,hCenterRadius,hSave, hAnalyze, hFilter, hDyeExcl],...
'Units','normalized');

axes(haCCD)
hCCDview=imagesc(current_data);
% Assign the GUI a name to appear in the window title.
set(f,'Name','Vesicle domain GUI')
% Move the GUI to the center of the screen.
movegui(f,'center')
% Make the GUI visible.
set(f,'Visible','on');

%-----------magnification window
```

```
    hpanel = imscrollpanel(f,hCCDview);

    set(hpanel,'Units','normalized','Position',[0.05 .1 .8 .8]);

     % Add the Magnification box.
     hMagBoxCCD = immagbox(f,hCCDview);

     % Position the Magnification box
     pos = get(hMagBoxCCD,'Position');
     set(hMagBoxCCD,'Position',[0 0 pos(3) pos(4)]);

     % Add the Overview tool.
     hovervw = imoverview(hCCDview);

  %----------------------------

%----------------MARK VESICLE CENTER AND BORDER------------------
    function CenterRadiusbutton_Callback(hObject,eventdata)
    % Mark center and radius of vesicle
    VN=VN+1;
    axes(haCCD)
    [centern(VN),centerm(VN)] = ginput(1); %mark center of vesicle
    [radiusn(VN),radiusm(VN)] = ginput(1); %mark radius of vesicle
    radius(VN) = sqrt((centern(VN)-radiusn(VN)).^2+(centerm(VN)-radiusm(VN)).^2);
    AreaVesicle(VN)=pi*radius(VN)*radius(VN);


    circx=(centern(VN)-radius(VN):0.01:centern(VN)+radius(VN));
    circy=abs(sqrt(-(circx-centern(VN)).^2+radius(VN)*radius(VN))+centerm(VN));
    circy_comp=-sqrt(abs(-(circx-centern(VN)).^2+radius(VN)*radius(VN)))+centerm(VN);

    hold on
    plot(centern(VN),centerm(VN),'.','LineWidth',4,'Color','green');
    plot(radiusn(VN),radiusm(VN),'.','LineWidth',4,'Color','green');
    plot(circx, circy, 'r','LineWidth',2),
    plot(circx, circy_comp, 'r','LineWidth',2)
    hold off

    end
%-------------------------------------------------------
```

```matlab
%--------ANALYSE VESICLES-----------------------------------------
function Analyzebutton_Callback(hObject,eventdata)

    Ftotal=zeros(VN,1);
    Gtotal=zeros(VN,1);

    for i=1:VN
        [Ftotal(i), Gtotal(i)]=gel_fluid_call(BW,centern(i), centerm(i), radi
    end



FTOTAL = sum(Ftotal);
GTOTAL = sum(Gtotal);
FRAC = [FTOTAL GTOTAL];
%set(haFrac);
haFrac = axes( 'Units','Normalized','Position',[0.85 0.1 0.15 0.20]);

haNumber = axes( 'Units','Normalized','Position',[0.85 0.3 0.15 0.20]);

VesicleDye=[DEN VN]; %[antal dyeexclusions, antal vesikler]

axes(haNumber)
bar(VesicleDye)



axes(haFrac)
pie([FTOTAL GTOTAL]);% colormap winter
title('Gel and fluid Fraction of Vesicles')
legend('fluid', 'gel')
end


% ----------------Filter DATA----------------
   function Filterbutton_Callback(hObject,eventdata)

   [BW]=vesicle_filtering_call(I, filter_radius);
   my_image_compare_tool(I,BW);
   filter_tjek = questdlg('Is filtering OK?','title','yes','no','yes');
```

```
    tjek = strcmp(filter_tjek, 'yes');

        if tjek == 1
            axes(haCCD)
            imagesc(BW);

            for i=1:DEN
                circxdye=(centerndye(i)-radiusdye(i):0.01:centerndye(i)+radiusdye(i)
                circydye=abs(sqrt(-(circxdye-centerndye(i)).^2+radiusdye(i)*radiusdy
                circy_compdye=-sqrt(abs(-(circxdye-centerndye(i)).^2+radiusdye(i)*ra

                hold on
                plot(circxdye, circydye, 'g','LineWidth',1),
                plot(circxdye, circy_compdye, 'g','LineWidth',1)
                hold off
            end

        else
            prompt={'state filter disk radius:'};
            dlg_title = 'Filter radius';
            num_lines = 1;
            %def = {5};
            filter_radius = inputdlg(prompt,dlg_title,num_lines);%,def);
            filter_radius=str2double(filter_radius);
        end
    close(hFig)
     end

%--------------Dye exclusion---------------

 function DyeExl_Callback(hObject,eventdata)

    % Mark center and radius of dye exclusion area
    %global circx, circy, circy_comp;
    DEN=DEN+1;
    axes(haCCD)
    [centerndye(DEN),centermdye(DEN)] = ginput(1); %mark center of vesicle
    [radiusndye(DEN),radiusmdye(DEN)] = ginput(1); %mark radius of vesicle
    radiusdye(DEN) = sqrt((centerndye(DEN)-radiusndye(DEN)).^2+(centermdye(DEN)-radiu
```

```
    circxdye=(centerndye(DEN)-radiusdye(DEN):0.01:centerndye(DEN)+radiusdye(DE
    circydye=abs(sqrt(-(circxdye-centerndye(DEN)).^2+radiusdye(DEN)*radiusdye(
    circy_compdye=-sqrt(abs(-(circxdye-centerndye(DEN)).^2+radiusdye(DEN)*radi

    hold on
    plot(circxdye, circydye, 'g','LineWidth',1),
    plot(circxdye, circy_compdye, 'g','LineWidth',1)
    hold off

    AreaDye(DEN)=pi*radiusdye(DEN)*radiusdye(DEN);

 end


% ----------------SAVE DATA----------------
   function Savebutton_Callback(hObject,eventdata)

    prompt={'state file name:'};
    dlg_title = 'Save';
    num_lines = 1;
    def = {'.mat'};
    profil_save = inputdlg(prompt,dlg_title,num_lines,def);
    profil_save=cell2mat(profil_save);

    save(profil_save, 'temp','I','BW','FRAC','VesicleDye','AreaVesicle','Area

   end

end
```

C.1.1   Filtering of vesicles

This program is called by the previous, and filters the image usig a diskstructure. The radius of this may be altered by the user.

```
%vesicle filtering

function [BWclean]=vesicle_filtering_call(I, filter_radius)

se=strel('disk',filter_radius);
```

```
Ibot=imbothat(I,se);
Isubbot=imsubtract(I, Ibot);

Iad=imadjust(Isubbot);


background = imopen(Iad,strel('disk',filter_radius));

I2 = imsubtract(Iad,background);

I3 = imadjust(I2);

level = graythresh(I3);

BW = im2bw(I3,level);

BWclean=bwmorph(BW,'clean');
```

C.2   Automated tether detection

The following program provides an example of applying the Hough transformation to an Image I using Matlab. It need the input image I, a black and white transformation BW of I, the number of tethers that should be detected, and the maximum gap allowed.

```
function hough_ren(I,BW,peaknumber, GAP)
%%%%start line detection------------------

%peaknumber =10; %numbers of peaks, i.e. estimate of number of tethers
global H T R P x y;

[H,T,R] = hough(BW,'ThetaResolution', 0.1, 'RhoResolution', 0.2);
figure,
imshow(H,[],'XData',T,'YData',R,...
          'InitialMagnification','fit');

 xlabel('\theta'), ylabel('\rho');
axis on, axis normal, hold on;
```

```
P  = houghpeaks(H,peaknumber, 'threshold',ceil(0.3*max(H(:))));
x = T(P(:,2));  %angles
y = R(P(:,1));
plot(x,y,'s','color','white');
colormap(jet), colorbar;

% Find lines and plot them
lines = houghlines(BW,T,R,P,'FillGap',GAP,'MinLength',1);
domain_length=zeros(1,length(lines));

figure,
imshow(I,[]), colormap(hot), hold on

for k = 1:length(lines)
   xy = [lines(k).point1; lines(k).point2];
   plot(xy(:,1),xy(:,2),'LineWidth',2,'Color','green');
    % Determine the length of line segment
   domain_length(k)=norm(lines(k).point1 - lines(k).point2); %length of gel d
end
```

C.3   Manual tether detection

The following program was used for manual tether detection. It operates on
a filtered image.

```
function tether_gui_scroll(I,temp)

current_data=I;

%global bwf_manbi;
global domain_nr domain_size;

scrsz = get(0,'ScreenSize');
   % Create and then hide the GUI as it is being constructed.
   f = figure('Visible','off','Position',[1 scrsz(4) scrsz(3) scrsz(4)]);
   % Construct the components.
  hCCD = uicontrol('Style','pushbutton','String','Show CCD image',...
          'Position',[scrsz(3)*0.95,scrsz(4)*0.95,120,25],...
```

```
        'Callback',{@CCDbutton_Callback});
hTeAZ = uicontrol('Style','pushbutton','String','Mark Tether',...
        'Position',[scrsz(3)*0.95,scrsz(4)*0.95-40,120,25],...
        'Callback',{@TeAZbutton_Callback});

hSave = uicontrol('Style','pushbutton','String','Save',...
        'Position',[scrsz(3)*0.95,scrsz(4)*0.95-80,120,25],...
        'Callback',{@Savebutton_Callback});


hAnalyze = uicontrol('Style','pushbutton','String','Analyze',...
        'Position',[scrsz(3)*0.95,scrsz(4)*0.95-120,120,25],...
        'Callback',{@Analyzebutton_Callback});




haCCD = axes('Units','Normalized','Position',[0.05 .1 .8 .8]);
%imshow(current_data, [], 'InitialMagnification', 'fit'), colormap(jet)
haTet = axes( 'Units','Pixels','Position',
[[scrsz(4)*0.95,scrsz(4)*0.1,60,scrsz(4)*0.7]]);

align([hCCD,hTeAZ,hSave, haTet, hAnalyze],'Center','None');

% Initialize the GUI.
% Change units to normalized so components resize
% automatically.
set([f,haCCD,hCCD,hTeAZ,hSave,haTet, hAnalyze],...
'Units','normalized');
%Create a plot in the axes.
%imshow(current_data, [], 'InitialMagnification', 'fit'), colormap(jet)
%imagesc(current_data)
axes(haCCD)
%imagesc(current_data);
hCCDview=imagesc(current_data);
% Assign the GUI a name to appear in the window title.
set(f,'Name','Tether domain GUI')
% Move the GUI to the center of the screen.
movegui(f,'center')
% Make the GUI visible.
set(f,'Visible','on');
```

```
%-----------magnification window

hpanel = imscrollpanel(f,hCCDview);

set(hpanel,'Units','normalized','Position',[0.05 .1 .8 .8]);

 % Add the Magnification box.
 hMagBox = immagbox(f,hCCDview);

 % Position the Magnification box
 pos = get(hMagBox,'Position');
 set(hMagBox,'Position',[0 0 pos(3) pos(4)]);

 % Add the Overview tool.
 hovervw = imoverview(hCCDview);

 %----------------------------

%----------------SHOW CCD PICTURE------------------
   function CCDbutton_Callback(hObject,eventdata)
   % Display surf plot of the currently selected data.
   axes(haCCD)
   imagesc(current_data);
   end
%-----------------------------------------------------


%-------------------MARK TETHER AND DOMAINS---------------
    function TeAZbutton_Callback(hObject,eventdata)
   % Display mesh plot of the currently selected data.
   [x_tether y_tether]=ginput(2); %mark start end end point of tether
    tether_length=  round(sqrt((x_tether(2)-x_tether(1)).^2 + (y_tether(2)-y_
    global bwf_manbi;
    bwf_manbi=zeros(tether_length,1);


    domain_length=zeros(100,1);
    k=1;
    axes(haTet)
    imagesc(bwf_manbi);
```

```
    man_tjek_nr=2;
    while man_tjek_nr==2;
        [x_man y_man] =ginput(2); %mark domain
        domain_start=  round(sqrt((x_man(1)-x_tether(1)).^2 + (y_man(1)-y_tether(1))
        domain_end=round(sqrt((x_man(2)-x_tether(1)).^2 + (y_man(2)-y_tether(1)).^2)

        domain_length(k)=round(sqrt((x_man(1)-x_man(2)).^2 + (y_man(1)-y_man(2)).^2)
        k=k+1;

        bwf_manbi(domain_start:domain_end,1)=1;

        %UPDATE BW TETHER AND IMAGE
        axes(haCCD)
        hold on
        plot(x_man(1),y_man(1),'.','LineWidth',2,'Color','green');
        plot(x_man(2),y_man(2),'.','LineWidth',2,'Color','green');
        hold off
        axes(haTet)
        imagesc(bwf_manbi), colormap(jet)

        domain_tjek = questdlg('more domains?','title','yes','no','yes');

        tjek = strcmp(domain_tjek, 'no');

        if tjek == 1
            man_tjek_nr=3;
        end

     end
    end
% ----------------SAVE PROFILE----------------
    function Savebutton_Callback(hObject,eventdata)
    global bwf_manbi;

    prompt={'state file name:'};
    dlg_title = 'Save';
    num_lines = 1;
    def = {'.mat'};
    profil_save = inputdlg(prompt,dlg_title,num_lines,def);
    profil_save=cell2mat(profil_save);
    save(profil_save,'temp', 'I','bwf_manbi', 'domain_nr', 'domain_size','-mat');
```

```
    end
%-------------------------------------------------
function Analyzebutton_Callback(hObject,eventdata)
    global bwf_manbi;
    [domain_nr, domain_size]=tether_analyzer(bwf_manbi);
end


end
```

C.3.1 Tether analysis

The program "tether analyzer.m" is called by the previous program, and analyses the extracted tether profile.

```
function [domain_nr, domain_size]=tether_analyzer(T)

tether_length=length(T);

domain_edges=zeros(2,100);
domain_nr=0;

for t=1:tether_length-1
    if T(t)~=T(t+1)
        if T(t)==0
            domain_nr=domain_nr+1;
            domain_edges(1,domain_nr)=t;
        end
        if T(t)==1
            domain_edges(2,domain_nr)=t;
        end
    end
end

[GF] = hist(T,2);   %0's and 1's, i.e. fluid and gel

domain_size=domain_edges(2,1:domain_nr)-domain_edges(1,1:domain_nr);
```

```
figure,
subplot(2,2,[1 3])
imagesc(T)
subplot(2,2,2)
hist(domain_size)
subplot(2,2,4)
pie([GF(1) GF(2)]),legend('fluid', 'gel'),colormap winter
```

Bibliography

[1] Kazunari Akiyoshi, Ayako Itaya, Shin ichiro M. Nomura, Naoaki Ono, and Kenichi Yoshikawa. Induction of neuron-like tubes and liposome networks by cooperative effect of gangliosides and phospholipids. *Federation of European Biochemical Societies Letters*, 534:33–38, 2003.

[2] J.-M. Allain, C. Storm, A. Roux, M. Ben Amar, and J.-F. Joanny. Fission of a multiphase membrane tube. *Physical Review Letters*, 93(15):158104, 2004.

[3] M. I. Angelova and D. S. Dimitrov. Liposome electroformation. *Faraday Discussions*, pages 303–+, 1986.

[4] L. A. Bagatolli and E. Gratton. Two-photon fluorescence microscopy observation of shape changes at the phase transition in phospholipid giant unilamellar vesicles. *Biophys. J.*, 77(4):2090–2101, 1999.

[5] Matthias Fidorra. Untersuchung des phasenverhaltens von membranen durch konfokale mikroskopie und kalorimetrie. Master's thesis, Institut für Schwingungsphysik der Georg-August-Universität zu Göttingen, 2004.

[6] Puzzle for children. *Produced by "Djeco"*, picture downloaded from www.gladeunger.dk.

[7] Agnieszka E. Hac, Heiko M. Seeger, Matthias Fidorra, and Thomas Heimburg. Diffusion in Two-Component Lipid Membranes–A Fluorescence Correlation Spectroscopy and Monte Carlo Simulation Study. *Biophys. J.*, 88(1):317–333, 2005.

[8] Thomas Heimburg. Mechanical aspects of membrane thermodynamics - estimation of mechanical properties of lipid membranes close to the chain melting transition. *Biochim. Biophys. Acta*, 1415:147–162, 1998.

[9] Thomas Heimburg and Andrew D. Jackson. On soliton propagation in biomembranes and nerves. *PNAS*, 102(28):9790–9795, 2005.

[10] D. W. Hilgemann. Getting ready for the decade of the lipids. *Annual Review Of Physiology*, 65:697–700, 2003.

[11] E. Hodneland, A. Lundervold, S. Gurke, X. C. Tai, A. Rustom, and H. H. Gerdes. Automated detection of tunneling nanotubes in 3d images. *Cytometry Part A*, 69A(9):961–972, September 2006.

[12] Paul V.C. Hough. Machine scanning of nuclear emulsions and bubble-chamber pictures. 1959.

[13] J. Hurtig, B. Gustafsson, M. Tokarz, and O. Orwar. Electrophoretic transport in surfactant nanotube networks wired on microfabricated substrates. *Analytical Chemistry*, 78(15):5281–5288, 2006.

[14] K. Jacobson, O. G. Mouritsen, and R. G. W. Anderson. Lipid rafts: at a crossroad between cell biology and physics. *Nature Cell Biology*, 9(1):7–14, January 2007.

[15] Mattias Karlsson, Max Davidson, Roger Karlsson, Anders Karlsson, Johan Bergenholtz, Zoran Konkoli, Aldo Jesorka, Tatsiana Lobovkina, Johan Hurtig, Marina Voinova, and Owe Orwar. Biomimetic nanoscale reactors and networks. *Annual Review of Physical Chemistry*, 55(1):613–649, 2004.

[16] Jonas Korlach, Petra Schwille, Watt W. Webb, and Gerald W. Feigenson. Characterization of lipid bilayer phases by confocal microscopy and fluorescence correlation spectroscopy. *PNAS*, 96(15):8461–8466, 1999.

[17] A. G. Lee. Lipid phase-transitions and phase-diagrams .2. mixtures involving lipids. *Biochimica Et Biophysica Acta*, 472(3-4):285–344, 1977.

[18] A. G. Lee. Ion channels - a paddle in oil. *Nature*, 444(7120):697–697, December 2006.

[19] Yu-Cheng Lin, Keng-Shiang Huang, Jen-Ta Chiang, Chih-Hui Yang, and Tzung-Heng Lai. Manipulating self-assembled phospholipid microtubes using microfluidic technology. *Sensors and Actuators B: Chemical*, 117(2):464–471, October 2006.

[20] N. Mahajan, Y. Zhao, T. Du, and J. Fang. Nanoscale ripples in self-assembled lipid tubules. *Langmuir*, 22(5):1973–1975, 2006.

[21] O G Mouritsen and M Bloom. Mattress model of lipid-protein interactions in membranes. *Biophys. J.*, 46(2):141–153, 1984.

[22] Shin-ichiro M. Nomura, Yumi Mizutani, Kimio Kurita, Akihiko Watanabe, and Kazunari Akiyoshi. Changes in the morphology of cell-size liposomes in the presence of cholesterol: Formation of neuron-like tubes and liposome networks. *Biochimica et Biophysica Acta (BBA) - Biomembranes*, 1669(2):164–169, May 2005.

[23] A. Roux, D. Cuvelier, P. Nassoy, J. Prost, P. Bassereau, and B. Goud. Role of curvature and phase transition in lipid sorting and fission of membrane tubules. *Embo Journal*, 24(8):1537–1545, April 2005.

[24] D. Schmidt, Q. X. Jiang, and R. MacKinnon. Phospholipids and the origin of cationic gating charges in voltage sensors. *Nature*, 444(7120):775–779, December 2006.

[25] Heiko M. Seeger, Marie L. Gudmundsson, and Thomas Heimburg. The influence of anesthetics, neurotransmitters and antibiotics on the relaxation processes in lipid membranes, 2007.

[26] S.J. Singer and G. L. Nicholson. The fluid mosaic model of the structure of cell membranes. *Science*, 175:720–731, 1972.

[27] A. J. Storkey, N. C. Hambly, C. K. I. Williams, and R. G. Mann. Cleaning sky survey data bases using hough transform and renewal string approaches. *Monthly Notices of the Royal Astronomical Society*, 347(1):36–51, 2004.

[28] Istvan P. Sugar, Thomas E. Thompson, and Rodney L. Biltonen. Monte carlo simulation of two-component bilayers: Dmpc/dspc mixtures. *Biophys. J.*, 76(4):2099–2110, 1999.

[29] C. Tanford. *The Hydrofobic Effect*. New York : Wiley, 1973.

[30] I. Tasaki. Evidence for phase transition in nerve fibers, cells and synaps. *Ferroelectrics*, 220, 1999.

[31] web.jjay.cuny.edu. internet.